

Received Date : 25-Mar-2014

Revised Date : 17-Nov-2014

Accepted Date : 17-Dec-2014

Article type : Original Manuscript

## **Nature, origin and evolution of a Late Pleistocene incised valley-fill, Sunda Shelf, Southeast Asia**

FAISAL A. ALQAHTANI<sup>1\*§</sup>, HOWARD D. JOHNSON<sup>1</sup>, CHRISTOPHER A-L. JACKSON<sup>1</sup>, and M.  
RAPI B. SOM<sup>2</sup>

*\*email: falqahtani@kau.edu.sa*

*or*

*f.alqahtani06@imperial.ac.uk*

*<sup>1</sup>Basins Research Group, Department of Earth Science & Engineering, Imperial College,  
London, SW7 2BP, UK*

*<sup>2</sup>PETRONAS Research Snd. Bhd., Bangi, 43000 Kajang, Selangor, Malaysia*

*<sup>§</sup>Current Address: Department of Petroleum Geology & Sedimentology, Faculty of Earth  
Sciences, King Abdulaziz University, P. O. Box 80207, Jeddah 21589, Saudi Arabia*

### **Short title – Evolution of a Late Pleistocene incised valley fill**

This is an Accepted Article that has been peer-reviewed and approved for publication in the *Sedimentology*, but has yet to undergo copy-editing and proof correction. Please cite this article as an “Accepted Article”; doi: 10.1111/sed.12185

This article is protected by copyright. All rights reserved.

## **ABSTRACT**

Understanding the stratigraphic fill and reconstructing the palaeo-hydrology of incised valleys can help to constrain those factors that controlled their origin, evolution and regional significance. This is addressed through the analysis of a large (up to 18 km wide by 80 m deep) and exceptionally well-imaged Late Pleistocene incised valley from the Sunda Shelf (South China Sea) based on shallow three-dimensional seismic data from a large (11 500 km<sup>2</sup>), 'merge' survey, supplemented with site survey data (boreholes and seismic). This approach has enabled the characterisation of the planform geometry, cross-sectional area and internal stratigraphic architecture, which together allow reconstruction of the palaeo-hydrology. The valley-fill displays five notable stratigraphic features: (i) it is considerably larger than other seismically-resolvable channel forms and can be traced for at least 180 km along its length; (ii) it is located in the axial part of the Malay Basin; (iii) the youngest part of the valley-fill is dominated by a large (600 m wide and 23 m deep), high-sinuosity channel, with well-developed lateral accretion surfaces; (iv) the immediately adjacent interfluves contain much smaller, dendritic channel systems, which resemble tributaries that drained into the larger incised valley system; and (v) a *ca* 16 m thick, shell-bearing, Holocene clay caps the valley-fill. The dimension, basin location and palaeo-hydrology of this incised valley leads to the conclusion that it represents the trunk river, which flowed along the length of the Malay Basin; it connected the Gulf of Thailand in the north with the South China Sea in the south-east. The length of the river system (>1200 km long) enables examination of the upstream to downstream controls on the evolution of the incised valley, including sea-level, climate and tectonics. The valley size, orientation and palaeo-hydrology suggest close interaction between the regional tectonic framework, low-angle shelf physiography and a humid-tropical climatic setting.

## **KEYWORDS**

Fluvial systems, incised valley, Malay Basin, sea-level change, seismic geomorphology, Sunda Shelf.

## **INTRODUCTION**

Incised valleys are large, fluvially-eroded geomorphological elements that are typically much wider (for example, up to several kilometres) and deeper (for example, up to several tens of metres) than single river channel forms (Schumm, 1993; Dalrymple et al., 1994; Schumm & Ethridge, 1994; Zaitlin et al., 1994; Hampson et al., 1997; Reynolds, 1999). Incised valleys are well-known for their role in transporting sediment to the shelf edge and deep sea during sea-level lowstands (Vail et al., 1977; Zaitlin et al., 1994); their erosional bases commonly form regionally developed sequence boundaries (*sensu* Van Wagoner et al., 1988), with the overlying coarse-grained sandstones that commonly fill the valleys forming very important hydrocarbon reservoirs around the world (Van Wagoner et al., 1988; Zaitlin et al., 1994). Incised valley-fill deposits also contain important geological information concerning Earth history, most notably climatic and sea-level variations, and about periods of tectonic deformation of the Earth's surface (Dalrymple et al., 1994; Blum & Tornqvist, 2000).

Incised valleys have been recognised throughout the geological record (Dalrymple et al., 1994; Zaitlin et al., 1994). However, much of the understanding of their form, genesis and fill comes from the analysis of Quaternary incised valleys (e.g. Posamentier & Allen, 1993; Reynaud et al., 1999; Nordfjord et al., 2005; Green, 2009; Paquet, et al., 2010). These studies demonstrate that fluvial incision may be driven by one or more of the following factors: (i) relative base-level fall, including eustatic events; (ii) tectonic uplift driving a relative fall in base-level; (iii) climate change, which may lead to increased rainfall resulting in greater fluvial discharge and incision; and (iv) river

capture, which can result in increased discharge in composite fluvial systems (Schumm & Ethridge, 1994; Thorne, 1994; Posamentier, 2001).

In coastal settings, incised valleys are particularly sensitive to fluvial incision driven by eustatic falls in sea-level, which may result in exposure of the shelf and the shelf edge (e.g. Mitchum et al., 1977; Vail et al., 1977; Van Wagoner et al., 1988, 1990; Posamentier et al., 1992; Zaitlin et al., 1994; Emery & Myers, 1996). The size and geometry of fluvial incision can be extremely variable (Schumm & Ethridge, 1994) but might be controlled initially by the magnitude of the base-level fall, by initial offshore water depth and/or by the slope of the shelf (Van Wagoner et al., 1990; Posamentier & Allen, 1999; Zaitlin et al., 1994; Posamentier, 2001). During non-glacial periods, when the low-magnitude of sea-level fall is typically insufficient to expose the entire shelf and shelf-edge, the magnitude and location of fluvial incision may be determined by the geometry of the coastal prism (Talling, 1998). In these cases, rivers may incise up to a maximum of 20 to 70 m into preceding highstand coastal plain deposits (Talling, 1998). Recent experimental work supports previous observations that valley width and depth is controlled mainly by the rate and magnitude of local base level fall and by initial offshore water depth (Martin et al., 2011). Other studies have shown a linear relationship between the drainage basin size and incised valley cross-sectional area, concluding that the size of the drainage basin area may be a more critical parameter for incised valley dimensions (e.g. Mattheus et al., 2007; Mattheus & Rodriguez, 2011; Phillips, 2011). Darmadi et al. (2007) also concluded that climatically driven fluctuations in discharge are more important than the sea-level change in determining the width and depth of fluvial channels on the Sunda Shelf, Southeast Asia.

Although incised valleys have been studied extensively, the interplay between upstream and downstream controls on their dimensions is poorly understood. Similarly, long-term fluvial evolution in response to upstream and downstream variability (for example, climatic and base-level changes, and tectonics) is poorly constrained (Blum &

Törnqvist, 2000). Consequently, applying any of the numerous empirically-derived relationships that attempt to explain the size and morphology of incised valleys is problematic. This difficulty is exacerbated near the coast where the influence of sea-level on the graded river profile decreases, but where the influence of climate and tectonics on the graded river profile increases (Shanley & McCabe, 1994; Blum & Törnqvist, 2000).

Deposition within incised valleys may occur during any part of the relative base-level cycle (Dalrymple et al, 1994, 2006). However, conceptual models and observations from Holocene systems indicates that sediment bypass is greatest during periods of maximum base-level fall and valley cutting (Blum, 1994; Blum & Törnqvist, 2000), while estuarine conditions characterise subsequent periods of relative base-level rise, especially in the downstream portion of flooded valleys (Dalrymple et al., 1994; Posamentier & Allen, 1999; Zaitlin et al., 1994).

Despite the substantial body of knowledge on the formation of incised valleys, the stratigraphic architecture of ancient incised valley fills remains limited due to several factors. Perhaps one of the most significant is the large lateral (i.e. hundreds of km<sup>2</sup>) and vertical (i.e. tens of metres) extent of incised valleys, which dwarfs the scale of even the largest outcrops, apart from some rare exceptions (e.g. Van Wagoner et al., 1990). Similarly, the basin physiography of many ancient incised valley fills is often poorly understood or is represented by relatively simplistic geometrical models (Talling, 1998). In the subsurface, there frequently are data limitations due to poor resolution and/or areal coverage (for example, seismic reflection data and well data). Elsewhere, high-resolution data, such as that provided by high-resolution-type seismic surveys, is usually of limited areal coverage.

This study aims to address these issues in relation to an exceptionally well-imaged Late Pleistocene incised valley on the Sunda Shelf (western South China Sea; Fig. 1). More specifically, the study provides a seismic stratigraphic characterisation of this

large incised valley system, documenting its planform geometry, dimensions, cross-sectional area and internal stratigraphic architecture. These data are then used to reconstruct the palaeo-hydrology of the valley system and to consider the significance of the results in relation to the depositional and sequence stratigraphic evolution of the Sunda Shelf during the Late Pleistocene. The study is based on the shallow portion (<500 ms) of a high-resolution, large 'merge' three-dimensional seismic reflection dataset, supplemented by a high-resolution site survey dataset that includes platform borings and high-resolution seismic data. Integrating these data provides a unique opportunity to evaluate the form, fill, genesis and significance of a major incised valley. This study focuses on an incised valley that can be traced along its axis for at least 180 km, making it one of the longest directly imaged ancient incised valleys in the world. Evidence also suggests that this valley system can be traced further to the NNW and into the Gulf of Thailand (Miall, 2002; Fig. 1), which would define a valley system at least 260 km long. The dataset in this study area is both extensive and of high imaging quality, which enables a detailed 3D seismic geomorphological analysis to be undertaken. In addition, the study area covers one of the world's largest epicontinental seas, which allows examining the upstream to downstream controls on the evolution of the incised valley, including sea-level, climate and tectonics. The drainage basin size and palaeo-discharge have also been estimated in order to better understand these controls. Three factors make this incised valley system under investigation particularly noteworthy: (i) it was cut during the Late Quaternary Last Glacial Maxima (LGM) and was filled during the Holocene transgression; (ii) the drainage basin extended into a tectonically-active mountain belt; (iii) the total valley and drainage basin area had a pronounced north-south elongation, with a total length of *ca* 2500 km, which spanned subtropical to humid tropical climatic settings; and (iv) the high-quality 3D seismic data provide an exceptional opportunity for in-depth, palaeo-geomorphological analysis. This study

attempts to unravel the relative importance of sea-level, climate and tectonics in controlling the origin and infill of this regionally-significant incised valley system.

## **REGIONAL GEOLOGICAL SETTING**

### **Tectono-stratigraphic development of the Malay Basin**

The Malay Basin is situated in the centre of the Sunda Shelf, Southeast Asia (Fig. 1). The basin trends north-west/south-east and is 500 km long by 250 km wide. It is located between the Penyu and West Natuna basins to the south, and the Pattani Basin to the north (Hutchison, 1989; Madon et al., 1999; Morley and Westaway, 2006; Pubellier & Morley, 2014; Fig. 1). The basin formed as a result of transtension during the Late Eocene to Early Oligocene related to the collision of the Indian Plate with the Eurasian Plate, which was followed by a period of post-rift thermal subsidence (Tapponnier et al., 1986; Hutchison, 1989; Pubellier & Morley, 2014). The rift to post-rift succession overlies pre-Tertiary metamorphic, igneous and sedimentary 'basement' (Figs 2 and 3). The Eocene–Oligocene syn-rift succession is 2 to 4 km thick and comprises mainly fluvial and lacustrine sediments that were deposited in one of several isolated, continental basins extending across much of Southeast Asia. In the Malay Basin the overlying post-rift succession is unusually thick (6 to 12 km) and comprises fluvial to deltaic and coastal Early Miocene to Recent deposits (Leo, 1997; Morley & Westaway, 2006). During the post-rift period, initially isolated syn-rift basins became linked and better connected, which caused rivers to form larger, through-going drainage systems (e.g. Leo, 1997; Morley & Westaway, 2006). For example, the Malay Basin became connected to the Pattani Basin to the northwest, with fluvial successions in the north-west passing basinwards into coastal-deltaic and marine successions to the south-east (Madon, 1999; Madon et al., 1999; Morley & Racey, 2001). The palaeo-Chao Praya River was one such linked fluvial–deltaic system (Leo, 1997).

The structural evolution of the Malay Basin can be divided into three tectono-stratigraphic phases (Tjia, 1994; Negah et al., 1996; Tjia & Liw, 1996; Madon, 1998;): (i) a pre-Miocene syn-rift phase, during which subsidence was controlled by normal faulting and sedimentation was characterised by deposition of fluvio-lacustrine sequences within isolated half-grabens (Hamilton, 1979; Madon, 1999); (ii) an Early to Middle Miocene post-rift phase, when a coastal plain-to-shallow marine environment was widespread and when thermally-induced, subsidence was dominant, followed by a subsequent period of basin inversion in which the most severe uplift occurred in the southern part of the basin, causing the south-western flank of the Malay Basin to be slightly steeper than its north-eastern flank (Fig. 3) (Madon, 1999); and (iii) a Late Miocene to Recent phase characterised by thermally-induced subsidence but lacking basin inversion (Fig. 3) (Madon et al., 1999). Deposition during this latter phase occurred mainly within a coastal plain to shallow marine environment (i.e. the Pilog Formation; Madon, 1999).

### **Physiography, palaeoclimatology and palaeohydrology of the Sunda Shelf**

The Sunda Shelf has an area of *ca* 125 000 km<sup>2</sup>, which makes it the largest epicontinental shelf in the world located within a tropical humid climate setting (Hanebuth & Stattegger, 2003; Hanebuth et al., 2011; Fig. 1). The Sunda Shelf can be considered an end member shelf-type by virtue of: (i) its extreme width (for example, 1000 km between the Mekong delta in southern Vietnam and the Rajang delta in south-west Borneo); (ii) the very low gradient of most of the shelf area (<0.01 degree); (iii) exceptionally high rates of sediment supply, with some of the highest sediment discharge rates in the world (Milliman et al., 1999); and (iv) the highest biodiversity in the world (Hanebuth et al., 2011).



During the Plio-Pleistocene, the Sunda Shelf was tectonically stable (Madon, 1998). The study area is located close to the Equator and near the 'West Pacific Warm Pool', which suggests that the Pleistocene climate, including the Last Glacial Maximum (LGM), was similar to the tropical climate of modern Southeast Asia lowlands (Morley, 2000; Sun et al., 2000). However, monsoon-driven precipitation during the LGM was lower than during the Holocene, suggesting that vegetation patterns in lowland areas, such as the Sunda Shelf, were potentially affected by the dry winter-monsoon (Wang et al., 1999).

The present-day water depth within the study area ranges from 50 to 80 m and the average water depth across most of the Sunda Shelf is *ca* 70 m. The shelf break occurs at *ca* 180 to 220 m beneath present-day sea-level, which is located *ca* 700 km to the east of the study area (Fig. 1). During the middle Pleistocene, the growth of continental glaciers decreased the volume of water in the world's oceans and, during the LGM, caused a maximum reduction in sea-level of *ca* 120 to 130 m (Gascoyne et al., 1979; Hopkins, 1982; Yang & Xie, 1984; Voris, 2000; Hanebuth et al., 2003; Hanebuth & Stattegger, 2003). Hence, most of the Sunda Shelf was subaerially exposed during the LGM, with the coeval shoreline located close to the present submerged shelf break (Voris, 2000; Hanebuth et al., 2003; Hanebuth & Stattegger, 2003). Consequently, the South China Sea was smaller during the LGM than it is at present, forming a semi-enclosed marginal sea with a 'blind gulf' type morphology (Sathiamurthy & Voris, 2006). The head of this gulf was located between south-west Borneo and the Malay Peninsula (Fig. 1), with the mouth of the gulf facing the Pacific Ocean, towards the north-east, in the area of the Philippines.

The modern sea-bed of the Sunda Shelf comprises either remnants of Pleistocene deposits below the Holocene transgressive surface or a thin veneer of Holocene to modern mud and silt (Hanebuth et al., 2003). However, during the Late Pleistocene most of the Sunda Shelf was exposed and was dissected by several major rivers. The ancestors

of the majority of modern SE Asian rivers have some sea-bed or shelf slope expression, which reflects their pre-Holocene, lowstand courses. For example, sea-bed bathymetry maps and shelf-edge canyons help to define the following rivers: palaeo-North Sunda (or Molengraaff) (Hanebuth & Stattegger, 2003; Wong et al., 2003), palaeo-Baram (Hiscott, 2003), palaeo-Padas in Brunei Bay (Sandal, 1996); and palaeo-Mahakam (Roberts & Sydow, 2003), among others.

Based on an analysis of present-day bathymetric contours, Voris (2000) and Sathiamurthy & Voris (2006) estimated the area of the Sunda Shelf that was exposed during the Pleistocene to Recent sea-level lowstand. These maps highlight several major submerged valleys, or palaeo-‘trunk’ river systems flanked and fed by tributary systems, most notably the following: (i) Mekong; (ii) Chao Phraya-Johore; (iii) Siam; (iv) North Sunda; (v) Rajang; and (vi) East Sunda. These valleys are typically expressed as elongate depressions on the modern sea floor, which are several hundred kilometres long. One of these major trunk rivers was termed the ‘Johore River’ by Voris (2000), which connected northwards with the ‘palaeo-Chao Phraya River’ of Morley & Westaway (2006). This river, which herein will be referred to as the ‘palaeo-Chao Phraya-Johore River’, ran south-eastwards through the Gulf of Thailand, along the axis of the Malay Basin and ultimately into the South China Sea (at the head of the gulf during the Late Pleistocene). Hence, the palaeo-Chao Phraya-Johore River represented one of the major ancient sediment conduits during the Late Pleistocene, which linked the Malay Basin and Sunda Shelf to a large drainage basin (*ca* 1 350 000 km<sup>2</sup>) that was located in the northern part of Thailand. In addition, the Malay Basin received sediment delivered by eastward-flowing rivers that drained the Malay Peninsula to the west (Loe, 1997; Morley & Westaway, 2006). Although the regional projection of this, and other large ‘trunk’ rivers, is reasonable, their precise location is uncertain due to the predominantly Holocene sedimentary cover and the sinuous nature of these river systems (Voris, et al., 2000). Direct imaging of these trunk rivers has yet to be achieved.

This article is protected by copyright. All rights reserved.

Based on a reconstruction of the clastic mass accumulation on the continental margins of Southeast Asia, derived from well logs, seismic profiles and from data published by Métivier et al. (1999), Clift (2006) concluded that sediment supply to Sunda Shelf from the Gulf of Thailand area declined during the Late Miocene to Recent and especially during the LGM. Hutchinson (1989) suggested that, during the Miocene, basins located south of the Gulf of Thailand, including the Malay Basin, received large quantities of material derived from rising mountain belts such as the Himalayas. It has also been suggested that the palaeo-Mekong River flowed through the Malay Basin during much of the Cenozoic, until it was diverted eastward along its present course in response to Late Cenozoic faulting (Hutchinson, 1989).

## **DATASET AND METHODOLOGY**

### **Three-dimensional seismic reflection data**

This study utilises a time-migrated 3D seismic reflection dataset that has a total areal extent of *ca* 11 500 km<sup>2</sup> (*ca* 115 km wide by *ca* 100 km long; Fig. 4). The seismic dataset comprises ten separate seismic surveys that have been merged into a single interpretable 3D volume (so-called 'merge' survey). The dataset is zero-phase processed with SEG normal polarity, in which a positive (peak) event (black seismic reflection on seismic sections) represents a downward increase in acoustic impedance, and a negative (trough) event (white seismic reflection on seismic sections) represents a downward decrease in acoustic impedance (Brown, 2004). In-line and cross-line spacing is 9.38 m and 12.5 m, respectively, and the vertical record length is 600 milliseconds two-way time (ms TWT). The vertical sampling interval for all surveys included in the merge is 2 ms, except for one survey which has a sampling interval of 1 ms. Although the data is time-migrated, and only sparse well data are available (see below), depth and thickness measurements are converted from ms TWT to metres by using velocity information (i.e. check-shot data) from a well (Tunggal-1; Fig. 4) that contains these data in the interval of

interest. This well indicates that the average velocity of the shallow part of the basin fill is *ca* 1880 m sec<sup>-1</sup>. Based on an estimate of the dominant seismic frequency (60 to 70 Hz) and velocity, the vertical resolution within the interval of interest ranges from *ca* 6.7 to 7.8 m and the lateral resolution ranges from *ca* 11.5 to 15.5 m; this allows the identification and mapping of even relatively small fluvial channel systems with a high degree of accuracy using seismic time-slices (*sensu* Zeng et al., 1998; Brown, 2003; Posamentier et al., 2007).

The quality of the seismic data within the studied interval is generally excellent, although exact amplitude values vary between different surveys due to variations in the acquisition and processing parameters. Fortunately, this does not unduly hamper the overall imaging and mapping of fluvial systems (Figs 5 and 6). There are also marked acquisition footprints in the upper parts of several of the individual datasets within the merge survey. These acquisition artefacts appear as amplitude stripes on horizontal seismic (time) slices (see below) and as small breaks or discontinuities along reflection events in seismic cross-sections. Finally, some of the individual surveys within the merge survey have not been optimally merged as evidenced by relatively minor (<4 ms), but abrupt vertical offset of reflection events. In addition, seismic 'multiples' from shallower channels may mask channels imaged at lower stratigraphic levels. However, through analysis of a combination of seismic sections and time-slices, only true geological features were interpreted.

### **Measuring morphometric parameters using geographic information system methodology**

Standard seismic interpretation and visualisation software are not designed to allow extraction of quantitative, spatially-referenced data from seismic reflection volumes. Therefore, seismic interpretation software has been integrated with geographic

information system (GIS) software to develop a methodology that can be used to measure and document the various geometric parameters of the studied fluvial systems. In particular, dataset limitations notwithstanding, the interpretive maps are treated as 'palaeo-satellite', Google Earth-type images, and they have been imported into ArcGIS for quantitative analysis. A semi-automatic data extraction workflow has been developed and can be found in Alqahtani (2010) (see also Kiel & Wood, 2011, 2012).

The morphometric parameters examined in this study include channel width (*CW*), channel depth (*CD*), meander belt width (*MBW*), meander wavelength (*ML*), channel length (*La*), sinuosity (*SI*) and radius of curvature (*RC*). All of these parameters have been determined using interpretative maps (time-slices) in ArcGIS (see Alqahtani, 2010). The exception to this is depth, which was measured directly from vertical slices through the seismic volume. The geometry of the channels has been documented and the associated parametric data has been used to estimate the palaeo-discharge of the channel and the valley (see Alqahtani, 2010 for all quantitative data used in the study). In addition, the drainage basin area has been estimated.

### **Site survey data**

#### *Platform borings and geotechnical cores*

Textural descriptions of bulk lithology from 16 platform borings were utilised in the present study. These platform borings are 30 to 150 m in length and provide information on the stratigraphic fill of the incised valley (Table 1 and Fig. 4). However, these reports were of different vintages (1974 to 2004) and of variable detail and quality. Because these data were primarily used for site investigation purposes, descriptions of the penetrated lithologies focused on sediment texture and geotechnical properties. Nonetheless, the textural descriptions of these cores were extremely useful and were fully utilised in this study. Most importantly, these data provide continuous lithological information from around 3 m below the seabed to the total depth of the borehole. An

idealised log has been produced, which combines information on the bulk lithologies and sedimentological characteristics of the 150 m thick stratigraphic interval of interest (Fig. 7). This log was tied to the seismic data using time-depth data in order to determine the lithology, calibrate this with seismic facies characteristics, including the high-resolution seismic data (Figs 7 and 8), and infer the depositional facies within and outside the incised valley fill.

#### *High-resolution seismic data (Boomer Data)*

High-resolution, Boomer-type seismic data are analogous to seismic reflection data but have a dominant frequency range of 2 to 7 kHz (compared to 250 Hz for the high-resolution 2D seismic data and 60 to 70 Hz for the 3D seismic data). These data provide very high-resolution images (vertical resolution of *ca* 3 to 5 m) of the internal stratigraphic architecture of the uppermost part (maximum of 60 m below seabed) of the incised valley (Fig. 8).

#### *Side-scan sonar and eco-sounder data*

Side-scan sonar and eco-sounder data provide detailed water depth information and images of seabed irregularities that may be related to differential compaction of the Holocene mud drape across shallowly-buried, pre-Holocene fluvial channels and valleys.

## **RESULTS**

Based on seismic facies variations, the Pleistocene to Recent succession of the Malay Basin has been divided into eight main seismic units (Units 1 to 8; Fig. 5) (Alqahtani, 2010). The horizons bounding these units have been mapped throughout the study area (Horizons A to H; see Tables 2 and 3, Figs 5 and 6). This study focuses on Units 6, 7 and 8 (Fig. 6). Based on the identification of marked vertical changes in seismic facies and lithology, Unit 7, which represents the main fill of the incised valley, has been sub-

divided into three sub-units (7.1, 7.2 and 7.3; Table 3, Fig. 6). The geometry, seismic character and distribution of channels and valleys within the constituent sub-units of Unit 7 are described below. In addition, the corresponding sedimentological character of these units is described, based on data derived from the platform borings and shallow cores.

## **Unit 6**

The base of Unit 6 is defined by Horizon E. This is a high-amplitude reflection event along which 'V'-shaped channels are developed. These channels are up to 32 ms twt (30 m) deep (Figs 5 and 6). In plan-view, these channels are 300 to 1300 m wide and of low to very low-sinuosity ( $SI = 1.0$  to  $1.3$ ; Fig. 9A). The majority of channels trend north-west/south-east and, based on the overall basinal context, are interpreted to have flowed south-eastwards (i.e. towards the South China Sea). In the middle of the study area, a 22 ms twt (20 m) deep by 1 km wide channel is observed that increases slightly in sinuosity eastwards (from  $SI = 1$  to  $SI = 1.2$ ). In addition, in the southern part of the study area, several very low to low-sinuosity channels ( $SI = 1$  to  $1.15$ ) are identified. These channels are 400 to 700 m wide and 12 to 15 m deep. Within Unit 6, above the basal channel systems described above, channels are typically narrower (maximum width of 320 m) and more sinuous ( $SI = 1.3$  to  $1.5$ ; Fig. 9B). These channels are characterised by 'V'-shaped and 'U'-shaped geometries in cross-section (Figs 5 and 6). In the middle of the study area, these channels are partly eroded by the valley developed at the base of Unit 7 (see below).

The lithology of the channels within Unit 6 is unknown because they are not penetrated by platform borings. However, platform boring data indicate that units adjacent to the channels are dominated by very stiff, dark-grey, silty clays that contain thin (<1 m) layers of fine-grained sand (Fig. 7B). These data also indicate that shell fragments are common in the middle part of Unit 6. The upper part of Unit 6, directly

beneath Horizon F and the adjacent interfluves of the valley developed at the base of Unit 7, is characterised by stiff, dark greenish-grey, silty-clay, with traces of organic material.

### **Unit 7**

The base of Unit 7 is defined by a high-amplitude reflection (Horizon F), along which a broad (13 km wide), deep (83 ms twt or 80 m), north–south trending, ‘U’-shaped valley is developed in the middle of the study area (Fig. 6). The margins of the valley are relatively steep (25 to 30°) and smooth although, on the valley interfluves, a low-angle (6 to 7°), low-relief (maximum of 18 to 23 m) erosional surface, which dips in towards the main valley, is developed. The width of this low-relief erosional ‘terrace’ increases southwards (from 16 to 18 km). Horizon F truncates reflections within Unit 6 and locally results in the complete removal of some of the channel systems within this underlying unit (Fig. 6). The magnitude of incision at the base of the valley is constant along the axis (i.e. along-dip) of the valley. Outside of the main valley, on the valley interfluves and on the low-relief erosional terrace described above, small (*ca* 50 m wide by <15 m deep), ‘V’-shaped channels are recognised (Fig. 6). In plan-view, these channels trend broadly perpendicular to and link in with the main north–south trending valley, although the mouths of these channels are located a considerable distance (up to 60 m) above the base of the valley as defined by Horizon F (Fig. 10A and B). These incisions have a pronounced dendritic pattern, with progressively smaller incisions branching off of larger incisions with increasing distance from the main valley-like incision (Fig. 10A and C). In the southern part of the study area, relatively deep [depth 17 to 34 ms twt (15 to 30 m)] and wide (width 400 to 900 m), low-sinuosity ( $SI = 1.1$ ), south-east flowing channels are developed (Fig. 10A and B).



As described above, Unit 7 displays a wide range of seismic facies and is characterised by a variety of lithologies. Based on these variations, this unit has been sub-divided into three sub-units: (i) 7.1; (ii) 7.2; and (iii) 7.3 (Fig. 6). These sub-units are described below.

#### *Sub-unit 7.1*

Sub-unit 7.1 is 12 to 15 ms twt (10 to 13 m) thick (Table 3). In cross-section, it is characterised by a series of chaotic, lenticular bodies (Fig. 6). Due to the poor imaging caused by seismic multiples generated by an overlying channel (see below), the plan-view morphology of these lenticular bodies is difficult to define.

Platform borings indicate that 75 m below the sea-bed and directly above the basal erosion surface (Horizon F), a 10 m thick unit of pebbles, gravel and cobbles is developed (see also Isa, et al. 1992; Fig. 7A). This unit is overlain by a 3 to 5 m thick unit of fine-grained sands. The 10 m thick, very coarse-grained unit and the overlying, 3 to 5 m thick sandstone unit appear to correspond to the chaotic, lenticular seismic facies described above (Figs 6 and 7A).

#### *Sub-unit 7.2*

Sub-unit 7.2 directly and conformably overlies sub-unit 7.1 and has an average thickness of 22 to 30 ms twt (20 to 28 m; Table 3). Over the majority of the study area, this sub-unit is characterised by laterally-continuous, flat-lying seismic reflections, although inclined reflections, which dip *ca* 7° and are up to 25 m high, are observed locally. Based on the spatial occurrence directly beneath geometrically identical features within the overlying sub-unit (7.3; Fig. 6), it is interpreted that these features represent seismic multiples and are not real geological features (see below).

Platform boring data indicate that sub-unit 7.2 broadly corresponds to a 15 to 20 m thick, shell fragment-bearing unit of fine-grained sands and very-stiff, silty-clays (Fig.

7A). This unit is overlain by a 5 to 8 m thick, very-stiff clay, which contains shell fragments towards its base and organic material towards its top (Fig. 7A).

### *Sub-unit 7.3*

Sub-unit 7.3 has an average thickness of 25-32 ms twt (23 to 30 m; Table 3). Internally, this sub-unit is dominated by a 27 ms twt (25 m) deep, 'V'-shaped, channel that is flanked by inclined (up to 7°) reflections which dip into towards the axis of the incision (Fig. 6). The channel is filled by low-amplitude seismic reflections. In plan-view, the 'V'-shaped incision represents a highly-sinuuous ( $SI = 2.8$ ) channel (Fig. 10A and D) that flowed south-eastwards. This channel is fully confined within the deep valley defined by Horizon F, is up to 600 m wide, and has a meander belt width of 13 km (Fig. 10B). The margins of the channel are, in many places, coincident with the steep valley walls (Fig. 6).

The detailed stratigraphic architecture and seismic facies of the highly-sinuuous channel is clearly imaged with the high-resolution seismic data (Fig. 8B). The high-resolution seismic data clearly defines the erosional base of the channel, which is 23 m deep. The basal part of the channel fill is characterised by an interval of high-amplitude reflections, which locally contains packages of chaotic, low-amplitude reflections (Fig. 8B). This interval is directly overlain by a package of alternating high-amplitude and low-amplitude reflections. Towards the top of the channel, low-amplitude, chaotic, and lenticular, high-amplitude reflections occur. Adjacent to the main channel fill (i.e. to the right-hand side of the high-resolution seismic section shown in Fig. 8), high-amplitude reflections, containing thin (1 m), packages of low-amplitude reflections, are developed.

Platform borehole data from the upper part of the channel indicate a 3 to 5 m thick, mud-clast conglomerate located at 40 m below the seabed, which corresponds to the base of the high-sinuosity channel in the upper part of the incised valley (i.e. in sub-

unit 7.3; Fig. 7A). This is overlain by a heterolithic unit comprising 15 to 18 m of interbedded fine sands and shell-bearing, stiff clays, which corresponds to the inclined reflections identified on the 3D seismic data (Fig. 8). The upper 2 to 3 m of the channel-fill is dominated by shell-bearing, stiff clays, within which scattered fragments of decayed wood are common.

### **Unit 8**

The base of Unit 8 is defined by Horizon G. Unit 8 has an average thickness of 17 to 20 ms twt (15 to 18 m) and is characterised by low-amplitude, laterally continuous seismic reflections. In map-view, no distinct geomorphological patterns are observed within this unit. On high-resolution seismic data, the lower part of Unit 8 is characterised by a 13 to 15 ms twt (11 to 13 m) thick package of low-amplitude, chaotic reflections, with lenses of high-amplitude reflections (Fig. 8). The upper part of Unit 8, directly below the seabed, is characterised by a 5 to 7 ms twt (3 to 5 m) thick package of high-amplitude, laterally continuous reflections, with lenses of low-amplitude, chaotic reflections.

Platform boring data indicate that a significant stratigraphic contact occurs 16 m below the seabed at the base of Unit 8. This contact is defined by a pronounced change in water content, with very-soft, water-rich (75 to 100%) clay below (in the upper part of unit 7.3), overlain by a 13 m thick, very-stiff, shell-rich, relatively water-poor (25 to 50%) clay (in the lower part of Unit 8; Fig. 7). The upper part of Unit 8 is dominated by coarse-grained, unconsolidated sands, which are interbedded with very-soft, wood fragment-bearing clays.

## **INTERPRETATION**

### **Pre-valley depositional patterns**

Unit 6 comprises the pre-incised valley depositional succession. It is interpreted to be composed of largely non-marine deposits, based on the abundance of seismically-imaged

channel systems (Ghosh et al., 2010) and its similarity with other Late Pleistocene fluvial successions described from other parts of Southeast Asia (Posamentier, 2001; Miall, 2002; Darmadi et al., 2007; Reijenstein et al., 2011). The predominant mud and silt lithologies, which are juxtaposed laterally against seismically-defined channels, imply a floodplain depositional environment (Fig. 7B). Channel trends remain consistent throughout Unit 6, (i.e. east to south-east), which suggests a hinterland located to the north-west and west, corresponding to the Gulf of Thailand area and the Malay Peninsula, respectively. In contrast, channel geometries are variable, changing from wider, lower-sinuosity forms in the lower part to narrower, higher-sinuosity forms in the upper part (cf. Fig. 9A and B). Based on conceptual models of fluvial system sequence stratigraphy (e.g. Schumm, 1993; Shanley & McCabe, 1993; Emery & Myers, 1996; Marriott, 1999), this gradual change in channel planform geometry could reflect an initial period of sea-level fall and lowstand, and formation of relatively straight, possibly braided fluvial systems, followed by a period of sea-level rise and highstand, and formation of relatively sinuously, meandering fluvial systems (Schumm, 1993; 2005). The basal part of Unit 6 resembles the wide, deep, low-sinuosity fluvial systems observed in the Java Sea, which are interpreted as the result of a moderate relative sea-level fall that was of insufficient magnitude to expose the entire Sunda Shelf ('lowstand bypass system' of Posamentier, 2001).

The abundant shell debris within the middle to upper part of Unit 6 indicates repeated marine incursions into an otherwise non-marine-dominated fluvial setting (Fig. 7B). In addition, the parallel, continuous, low-amplitude seismic reflections identified within the middle and upper parts of Unit 6 are consistent with a non-channelised, lower coastal plain to marginal marine depositional environment (Figs 5 and 6).

### **Incised valley interpretation**

Unit 7 is interpreted as a major incised valley. It is concluded that this forms part of the palaeo-Chao Phraya-Johore River, which was a major, through-going trunk river on the Sunda Shelf (see also *Physiography, palaeoclimatology and palaeohydrology of the Sunda Shelf* and following discussions).

The following diagnostic criteria have been used to aid the identification of incised valleys and to distinguish them from locally developed deep channels (see Hampson et al., 1997; Posamentier, 2001; Fielding & Gibling, 2005; Gibling, 2006; Best & Ashworth, 1997): (i) the basal erosion surface that records the lowstand of relative sea-level (sub-areal unconformity or sequence boundary) must be of regional (i.e. basin-wide) extent; (ii) the basal erosion surface truncates strata which are present beneath the adjacent interfluves; (iii) the basal surface may be associated with the presence of small tributaries on the main valley interfluves (Posamentier, 2001); (iv) the incised valley fill has a distinctive internal architecture that is commonly multi-storey and which records the progressive rise in base-level during the filling of the valley; (v) facies deposited within the incised valley are younger than those adjacent to and below the erosional surface and may display different facies and architectural characteristics; and (vi) the depth and width of the incised valley is significantly larger than expected for a 'normal' fluvial channel system (for example, several kilometres wide and several tens of metres deep; Zaitlin et al., 1994; Reynolds, 1999; Gibling, 2006).

When considering these criteria in light of the geomorphological element described here, it has been noted that the base of the valley is at least of sub-regional extent and covers at least 11 500 km<sup>2</sup> (Figs 1 and 4). The feature is also significantly deeper (up to 80 m) and wider (8 to 18 km) than a typical single-storey fluvial channel, such as those observed in sub-unit 7.3, which are typically <30 m deep and <1300 m wide (Fig. 6). The fluvial architecture and facies within the valley is also significantly

different to that developed outside of it. For example, the valley also has a complex stratigraphic fill, consisting of a basal coarse-grained interval (sub-unit 7.1), which is overlain by two heterolithic, shell-bearing intervals (sub-units 7.2 and 7.3), the uppermost of which is characterised by a large meandering channel system with well-developed point-bars and scroll cut-offs (Fig. 10). Small tributaries are developed on the areas immediately adjacent to the main valley-like incision, which most probably represent smaller fluvial channels formed during base-level lowering and valley incision. However, it is also possible that they could represent dendritic tidal channels draining tidal flats and linked to the later transgressive infill of the valley. Unfortunately, we cannot unequivocally distinguish between the two models based on the available data, but favour a tributary origin (Fig. 10C). The evidence of marine-influenced facies in the upper part of the valley fill would be consistent with a tidally-influenced channel interpretation (Dalrymple et al., 1992). Finally, the Unit 7 valley-confined deposits are capped by Holocene age, fully marine shelf mud deposits, which extend outside of the main valley axis and across the whole Sunda Shelf (Figs 6 and 7).

Hence, Unit 7 is interpreted as an incised valley formed due to a significant fall in relative sea-level (see Fig. 11) and Horizon F, which bounds the base of the valley, is interpreted as a sequence boundary (*sensu* Van Wagoner et al., 1988). This sequence boundary is characterised by a single, deep and wide incised valley. This contrasts with those documented elsewhere, where the sequence boundary is characterised by an amalgamation of multiple cycles and incised valleys of various ages are preserved next to each other, such as those in the eastern Gulf of Mexico (e.g. Mattheus & Rodriguez, 2007; Mattheus et al., 2011) and those on the New Jersey continental shelf (e.g. Nordfjord et al., 2005). The depth, width, regional extent, cobble-grade lag, its NNW-SSE orientation and basin-axis location are all consistent with the valley representing a major trunk river.

The seismically-defined incised valley is located <50 km to the south-west of the highly speculative location of the same river proposed by Sathiamurthy & Voris (2006) (Fig. 18C). The seismic dataset indicates no such valley to the south-west hence the position of the palaeo-Chao Phraya-Johore River, as shown on the maps of Sathiamurthy & Voris (2006), needs to be reassessed and placed on the axis of the Malay Basin (Fig. 18C).

### **Depositional evolution and stratigraphy of the incised valley**

The stratigraphic architecture of the incised valley fill is highly variable (Fig. 6) and we lack chronostratigraphic data to precisely define the age relationships of the various sub-units. The lowest unit, sub-unit 7.3, is a 13 m thick, relatively coarse-grained, upward-fining sequence developed at the base of the incised valley, which is interpreted as braided fluvial deposits that formed during initial lowstand conditions (Figs 7A and 12A) (cf. Fisk & McFarlan, 1955). The internal lenticular geometry may represent the seismic expression of multi-lateral channels and bars (e.g. Shanley & McCabe, 1994), such as those observed at the base of the Mississippi incised valley (Fisk & McFarlan, 1955).

The middle unit, sub-unit 7.2, is devoid of clear geomorphological patterns in the seismic data. Overall, it is characterised by an upward-fining succession, with a 15 to 20 m thick, shell-bearing unit of fine-grained sands and silty-clays (Fig. 7A), which is overlain by 5 to 8 m of shell-bearing, organic clay. Shell material is ubiquitous, which implies marine-influence, possibly associated with increasing base level. The heterolithic, fine-grained sands and silty-clays closely resemble tidally-influenced fluvial point bars within an estuarine depositional setting (Thomas et al., 1987). Hence, it has been interpreted that this stacking pattern represents the initial flooding of the valley due to rising base level (Fig. 12B) (Allen & Posamentier, 1993).

Sub-unit 7.3 represents the final fill of the valley, with deposition largely within, and adjacent to, a large meandering river (Figs 6 and 8). The 3 to 5 m thick, mud-clast conglomerate identified at the base of the channel is interpreted as a basal lag related to channel incision and lateral migration (Fig. 7A). The crescentic-shaped amplitudes located on the inner part of the river meanders are interpreted as scroll-bars formed by lateral migration of the river. The low-angle (5 to 7°) dipping reflections observed in cross-section adjacent to the main 'V'-shaped channel correspond to a 15 to 18 m thick interval of interbedded fine sands and shell-bearing, stiff clay and alternating high-amplitude and low-amplitude seismic reflections (Fig. 8). The dipping reflections probably represent lateral accretion surfaces that formed in response to lateral channel migration. The occurrence of meander-scrolls, lateral accretion surfaces, neck-cut offs and associated abandoned channel-fills are consistent with a meander-belt depositional setting (Figs 10A, 10B and 13). The upper 2 to 3 m of the channel-fill is dominated by shell-bearing clay and plant debris, which corresponds to low-amplitude, chaotic, and lenticular, high-amplitude seismic reflections. These fine-grained units document channel abandonment (Bridge, 2003).

The key elements of sub-unit 7.3 are the following: (i) the abundance of shell material; (ii) the heterolithic nature of the unit and the seismic and well data evidence for IHS; (iii) the occurrence of a large river within an incised valley; and (iv) the abundance of organic material. In addition, this interval is overlain by fully marine muds of the Holocene transgression and appears to be associated with the final phase of drowning of the valley. This is supported by the heterolithic, shell-rich nature of sub-unit 7.3, which implies a degree of marine influence (i.e. fully saline to mixed salinity conditions) and fluctuating energy levels during deposition. These conditions are typically found within tide-dominated or tide-influenced depositional systems (e.g. Thomas et al., 1987; Allen & Posamentier, 1993; Allen & Chambers, 1998).



Salt-water intrusion is common in many modern rivers, especially those with very low river gradients ( $<0.01^\circ$ ) and reduced stream discharge. Upstream salt-water intrusion in fluvial-estuarine systems is frequently controlled by the slope of the coastal plain, and can be several tens of kilometres in extent (Miall, 1996; see also incised valley 'segment 2' of Zaitlin et al., 1994). Salt-water intrusion is larger during the dry season at a time when the flux of freshwater is reduced. The distance of salt-water intrusion is up to 200 km in the modern Chao Phraya River and 150 km in the Rajang River (Woodroffe, 2000). For larger rivers that have large catchments and are associated with relatively steep coastal-plain gradients (for example, the Mekong River) salt-water intrusion may be reduced to 50 to 100 km (Woodroffe, 2000). In contrast, in a low-gradient system, such as the Amazon River, salt-water intrusion can reach 1000 km (Mertes & Dunne, 2007). The low-gradient Sunda Shelf was also conducive to a very large upstream salt-water intrusion, which would have been enhanced by the inferred lower monsoon-driven precipitation rates during the Pleistocene (Wang, et al., 1999).

During rising base-level, tributaries may have become tidally-influenced channels, either with or without upstream fluvial connections. The tributary-style channels seen in this example have a dendritic pattern and drain into the main channel (Fig. 10C). Tidal channels are common in the lower reaches of many modern rivers in Southeast Asia, specifically where the lower coastal or delta plain experiences a meso-tidal to macro-tidal range, such as in the Niger, Indus, Ganges-Brahmaputra, Irrawaddy, Mekong, Rajang, Padas, Mahakam and McArthur rivers, among others (e.g. Allen, 1965; Oomkens, 1974; Allen & Chambers, 1998; Nummedal et al., 2003; Sidi et al., 2003; Staub & Gastaldo, 2003; Tanabe et al., 2003; Kuehl et al., 2005; Jones et al., 2003). In these cases a high proportion of the channels are almost entirely tidal and only rarely connect with upstream fluvial channels.

The Holocene period witnessed final drowning of the incised valley and the capping (Unit 8) of the uppermost meandering channel (sub-unit 7.3) by marine clay (Fig. 12D). The present-day shoreline around the Malay Basin and Gulf of Thailand reflects the extent of the Holocene transgression and its impact on coastal depositional systems (Hanebuth et al., 2011). Only the Mekong River has been able to build a large (150 km wide) delta on the Sunda Shelf (initiated at *ca* 8.0 ka; Ta et al., 2002, 2005; Tamura et al., 2009). The majority of the Sunda Shelf, and the surrounding shorelines, are dominated by the effects of the Holocene transgression, despite the high rates of modern sediment supply (Hanebuth et al., 2011).

### **Drainage basin size**

The palaeogeography of the Late Quaternary Sunda Shelf area is relatively well constrained (Voris, 2000; Hanebuth et al., 2003; Hanebuth & Stattegger, 2003). The palaeo-Chao Phraya-Johore River drainage basin was flanked to the east and west by the Indo-China Block and the Malay Peninsula (Pubellier & Morley, 2014), respectively, and extended northwards into the present-day catchment area of the modern Chao-Phraya River (Morley & Westaway, 2006). Bathymetric maps and the seismic interpretations presented here show a consistent southwards-flowing trend of the main incised valley, along the axis of the Malay Basin (cf. Figs 1 and 4). Northwards extrapolation extends the valley system along the axis of the Pattani Trough/Gulf of Thailand Basin towards the valley of the modern Chao-Phraya River, onshore Thailand, which is dominated by Cenozoic fault systems (Morley & Westaway, 2006; Morley et al., 2011). Hence, the catchment area of the whole palaeo-Chao Phraya-Johore River valley probably included both the hinterland of Thailand (up to 2500 m relief) and the mountains of the Malay Peninsula (up to 800 m relief; see below for more detail) (Fig. 14). Consequently, the drainage basin area for the incised valley is estimated to have been *ca* 1 350 000 km<sup>2</sup>;

this suggests that the valley system was part of a large drainage basin, comparable to some of the world's largest (Table 4; Fig. 15).

The palaeo-Chao Phraya-Johore River drainage basin is much larger than most of the major rivers in the Southeast Asia, including the Mekong and Indus Rivers. It is also larger than the drainage basins that supplied incised valleys in the eastern Gulf of Mexico (Mattheus et al., 2007) and New Jersey (Nordfjord et al., 2005) (Table 6; Fig. 16). However, the palaeo-Chao Phraya-Johore drainage basin is smaller than the Brahmaputra River, (1,730,000 km<sup>2</sup>), whose drainage basin comprises the Himalaya Mountains, which also results in very high river gradients (Fig. 15 and Table 4). The drainage area of the palaeo-Chao Phraya-Johore River incised valley is most comparable, in terms of plan-view size, to the Orinoco River (1 330 000 km<sup>2</sup>), which is one of the top ten largest rivers in the world.

### **Palaeo-discharge analysis**

The high-quality seismic images presented here of both planform geometry and cross-sectional area enables the discharge of the palaeo-fluvial channels to be estimated by utilising empirical equations determined for modern rivers (Table 5). These equations enable estimation of the palaeo-discharge for individual channels, such as the meandering channel that is preserved in the upper part of the incised valley (sub-unit 7.3). This also allows comparison of the results of this study with the discharge of major rivers in Southeast Asia and elsewhere (Tables 4 and 5).

There are several relationships from modern rivers that relate the planform geometry [i.e. meander wavelength ( $ML$ ), channel width ( $CW$ )], cross-sectional area ( $A$ ) and channel slope ( $S$ ) to discharge ( $Q$ ) (Dury, 1976). These relationships can be divided into two groups based on the types of the fluvial channel (Table 5). Most of these equations are used for high-sinuosity channels. In addition, these equations are useful to estimate either the average or bankfull discharge.

The relationships described above have been applied to the clearly imaged meandering channel in sub-unit 7.3, where the wavelength is confidently constrained (ca 14 000 m). The equations of Leopold & Wolman (1957;  $ML = 65.2Q_b^{0.5}$ ) and Mackey (1993;  $ML = 65.2Q_b^{0.5}$ ) predict the bankfull discharge ( $Q_b$ ) for this channel may have been around 46 106 m<sup>3</sup>/s and 46 550 m<sup>3</sup>/s, respectively. However, the bankfull discharge estimated using the equation outlined by Sümeğhy & Kiss (2011) ( $Q = 0.0003ML^2 + 0.3440ML - 81.329$ ) yields 63 534 m<sup>3</sup>/s. The estimated discharge from using the equations above is the bankfull discharge. The average discharge ( $Q$ ) can be estimated using the equations of Carlston (1965;  $Q = 0.000017 ML^{2.15}$ ) and Osterkamp & Hedman (1982;  $Q = 0.027 CW_b^{1.69}$ ) yielding estimates of 13 952 m<sup>3</sup>/s and 1338 m<sup>3</sup>/s, respectively. The estimated average discharge derived from the equation of Carlston (1965) is based on meander wavelength ( $ML$ ), which is a more reliable measurement than channel width ( $CW$ ) and is used in the equation of Osterkamp & Hedman (1982).

The cross-sectional area ( $A$ ) approach to calculating fluvial bankfull discharge is based on equations presented by Dury (1976;  $Q_b = 9.93 A_b^{0.85}$ ) and Williams (1978;  $Q_b = 4.0 A_b^{1.21} S^{0.28}$ ); these estimate bankfull discharge of 35 207 m<sup>3</sup>/s and 31 144 m<sup>3</sup>/s, respectively. These estimated bankfull discharge values are lower but compare reasonably well with those derived from the planform geometry data.

The Manning equations (developed in 1889) are widely used to estimate bankfull discharge ( $Q_b$ ) [ $Q_b = (CW*CD)^{5/3} S^{1/2} (1.49/n)$  where  $CW$  = channel width,  $CD$  = channel depth,  $S$  = gradient, and  $n$  = Manning's roughness coefficient]. The gradient ( $S$ ) and roughness coefficient ( $n$ ) parameters can be easily determined for modern rivers, but this is not possible for the ancient rivers studied here since these parameters cannot be obtained directly from seismic reflection data. However, some studies have used the Manning's roughness coefficient ( $n$ ) of modern rivers in order to calculate the bankfull discharge of ancient rivers. Kiel & Wood (2011) used Manning's roughness coefficient

( $n$ ) for the Amazon River ( $n = 0.025$ ) because of its inferred analogy with their large, low-latitude, ancient rivers. In this study, the same Manning's roughness coefficient ( $n$ ) of Amazon River ( $n = 0.025$ ) has also been used because of similarities between the fluvial system identified in this study and that studied by Kiel & Wood (2011). Furthermore, and in order to calculate the discharge for the channel in sub-unit 7.3 using Manning's equation, an estimate of the gradient ( $S$ ) of the valley is required. The approach of Kiel & Wood (2011) in estimating the gradient ( $S$ ) (gradient is  $10^{-4}$ ) has been followed. Hence, the bankfull discharge estimate based on Manning's equations is estimated as  $36\,740\text{ m}^3/\text{s}$  for the meandering channel observed in sub-unit 7.3.

The estimated bankfull discharge of the meandering channel in sub-unit 7.3 (*ca*  $36,740$  to  $46,550\text{ m}^3/\text{s}$ ) is larger than any mean annual flood discharge value of all the major rivers in Southeast Asia (Tables 4 and 5). The discharge value of the meandering channel (sub-unit 7.3) is comparable to the Yangtze ( $31\,900\text{ m}^3/\text{s}$ ), and considerably larger than the Mississippi River ( $16\,200\text{ m}^3/\text{s}$ ). These high discharge values are consistent with both the inferred large size of the palaeo-Chao Phraya-Johore River's drainage basin and the humid tropical climate that characterised the catchment area.

## **DISCUSSION**

Following Schumm (2005), the main controlling factors of the palaeo-Chao Phraya-Johore River have been divided into three segments (Fig. 14): (i) up-stream controls, including tectonics, climate, lithology and the geological history; (ii) local (mid-stream) controls, including valley morphology, vegetation, active tectonics, tributaries and type of bedrock; and (iii) down-stream controls, which include base-level fluctuation and 'length' (i.e. how far upstream the effects of the base-level variations extend).

The up-stream segment of the palaeo-Chao Phraya-Johore River and associated catchment comprised the active mountain-belt of north Thailand (the eastern extension

of the Himalayas) which, at present, has up to 2500 m of relief. During the early part of the Neogene, most of Thailand was characterised by continental rift basins, which fragmented the continental drainage into small, disconnected fluvial systems (Morley & Racey, 2011). However, when rifting ceased and thermal subsidence commenced, these fluvial systems linked to form longer, through-going systems associated with significantly larger drainage basin areas, mainly due to tectonically-induced river capture. The course of the modern Chao Phraya and other rivers onshore Thailand continues to be strongly controlled by tectonics, with most rivers running parallel to the pervasive north-south striking Cenozoic fault systems. Similar processes operated intermittently throughout the Neogene onshore and offshore Thailand, resulting in several major southward-flowing trunk rivers that were fed by smaller tributaries draining adjacent hinterlands (Morley & Racey, 2011).

The mid-stream segment dominates the study area (Fig. 14). The closest hinterland is the Malay Peninsula, which sourced numerous smaller, easterly flowing rivers that are imaged in the western side of the dataset. These rivers were responding to a regional easterly tilt that was enhanced by a series of easterly-dipping fault systems (for example, the Western Hinge Fault Zone of the Malay Basin; Madon, 1999). The main axial trunk river (palaeo-Chao Phraya-Johore River) was always located to the east of this fault terrace and probably connects with the valley documented at a similar stratigraphic level by Miall (2002), which is located only 80 km immediately to the north/north-west. Regional subsidence analysis (Madon & Watts, 1998) and seismic geometries within the immediate study area and across the wider Malay Basin, suggests that the mid-stream area was tectonically quiescent during the Late Pleistocene. This argues against tectonics as the key driver for relative sea-level fall and incised valley formation.

The dataset indicates that the incised valley is at least 180 km long, which makes it one of the longest directly imaged ancient incised valleys in the world; furthermore, if

this assumption is correct in linking it to that described by Miall (2002) this valley system would be at least 260 km long. Following this trend further north-westwards, the palaeo-Chao Phraya River, in the eastern part of the upper Gulf of Thailand, is also located within an incised valley (Tanabe et al., 2003). The regional north-west/south-east orientation of the incised valley, and its location parallel to the axis of the Malay Basin (Maddon & Watts, 1998), supports regional subsidence as a large-scale control on the trend and position of this trunk river.

The down-stream segment of rivers is mainly controlled by base-level changes, as indicated by most sequence stratigraphic models (e.g. Van Wagoner et al., 1990; Schumm, 1993; Shanley & McCabe, 1994; Posamentier & Vail, 1998). Sea-level fall is also the most compelling driver for the formation of the Late Pleistocene valley identified here. During the Late Pleistocene, the Malay Basin and the larger palaeo-Sunda Shelf was characterised by a broad (up to 800 km), very low-gradient (*ca* 0.01°), shallow (50 to 80 m), periodically emergent shelf (Hanebuth & Stattegger, 2003; Hanebuth et al., 2011). Thus, a significant relative sea-level fall (*ca* 120 m; Fig. 11) was likely to expose all of the Sunda Shelf and to trigger fluvial incision and incised valley formation. Sea-level fluctuations are also manifested in changes in channel sinuosity, width and/or depth along a river's course (Blum & Törnqvist, 2000; Schumm, 2005). Meandering rivers often decrease in sinuosity downstream towards the coeval shoreline and this can be seen in the lower reaches of the channel in sub-unit 7.3 (Fig. 17C).

However, it is also likely that channel trends in the down-stream segment were also influenced by structure, as indicated by the sudden change from a south-eastwards to a north-eastwards channel flow direction (Figs 1 and 14). The latter coincides with the north-east/south-west Penyu Basin trend, which cross-cuts the previously dominant north-west/south-east Malay Basin trend of the mid-stream segment (Maddon & Watts, 1998). The Penyu Basin trend also influences other Pleistocene rivers in this area, such

as the Molengraaff or North Sunda River, which drained a separate hinterland dominated by southern Sumatra (Darmadi et al., 2007; Kiel & Wood, 2011 and 2012; Reijenstein et al., 2011).

The downstream segment is interpreted to be influenced by rising sea-level and by strong tides, with the latter enhanced by tidal amplification (Collins et al., 2014). This was promoted by the blind gulf at the south-western end of the South China Sea in the Late Pleistocene, with tidal amplification continuing today in the mouths of the Rajang, Mekong and Pahang rivers (Staub et al., 200; Ta et al., 2002; Zu et al., 2008; Razak et al., 2012). Manifestation of similar processes and environments in the study area comprise the transgressive, tide-influenced estuarine deposits that form the final stage of the palaeo-Chao Phraya-Johore valley-fill. Tide-influenced coastal systems are widespread in Southeast Asia due to the complex interaction between Pacific and Indian Ocean tides and by the highly compartmentalised basin physiography, which promotes tidal amplification (e.g. Nummedal et al., 2003). This is illustrated in numerous examples of tide-dominated areas, such as the Bay of Bengal (Ganges-Brahmaputra delta; Kuehl et al., 2005), Straits of Malacca (Klang-Langat delta; Coleman et al., 1970), Makassar Straits (Mahakam delta; Allen & Chambers, 1998) and Gulf of Papua (Fly delta; Dalrymple et al., 2003). Macro-tidal conditions also characterise nearby present-day river mouths around the periphery of the Sunda Shelf, most notably the Mekong (Unverricht et al., 2013; Zuo Xue et al., 2010), the Rajang (Staub et al., 2000; Staub and Gastaldo, 2003) and the Pahang (Razak et al., 2012). The results indicate that the drowned palaeo-Chao Phraya-Johore valley became a tidal estuary, which gradually migrated north-westwards, along the axis of the valley, due to accelerating sea-level rise during the Holocene. This could have been an important site for the northward migration of early humans, particularly since fossils of *Homo erectus* have been found in similar Plio-Pleistocene deposits around the periphery of the Sunda Shelf and in eastern Java (Huffman, 1999, 2001; Huffman & Zaim, 2003).



## CONCLUSIONS

1. A large, sub-regional merged three-dimensional seismic dataset (11 500 km<sup>2</sup>), supplemented by high-resolution site survey seismic and borehole data, has enabled reconstruction and quantification of Late Pleistocene fluvial systems in the Malay Basin at a level of detail not previously possible.
2. Two different types of fluvial channel incisions have been identified: (i) deep incised valley systems (up to 80 m deep and 8 to 18 km wide) are interpreted as the result of periods of major sea-level fall (100 to 120 m) when the shelf was widely exposed, and (ii) weakly incised channel systems (20 to 30 m deep and 0.3 to 1.3 km wide) are interpreted as lowstand alluvial bypass channel systems.
3. The largest and most prominent incised valley is interpreted to have formed during the Last Glacial Maximum (LGM) lowstand, when the sea-level had fallen to, or just below, the shelf-edge and when the majority of the extensive and low-gradient Sunda Shelf was exposed. Borehole data preserve a cobble layer at the base of the valley, which supports a high-energy fluvial origin, most likely to be coincident with the lowstand cutting of the valley.
4. This exceptionally large valley is thought to be part of the palaeo-Chao Phraya-Johore River, which was a major trunk river that originated in the highlands of northern Thailand, drained southwards through the Gulf of Thailand and the Malay Basin, and discharged into the South China Sea.
5. The drainage basin area palaeo-Chao Phraya-Johore River is estimated to have been *ca* 1 350 000 km<sup>2</sup>, which makes it larger than most of the major drainage basins of Southeast Asia and comparable in size to those of the world's largest present-day rivers. It was probably the largest drainage system in the Sunda Shelf area during the Pleistocene.
6. Estimates of the bankfull discharge, based on empirical relationships derived from modern rivers, suggests values ranging from *ca* 36 740 to 46 550 m<sup>3</sup>/s for the large

meandering river (in sub-unit 7.3). This is larger than many modern rivers in Southeast Asia and is comparable to the Yangtze (31 900 m<sup>3</sup>/s). These high discharge values are consistent with both the estimated drainage basin area and the humid tropical climate of the palaeo-Chao Phraya-Johore River.

7. The final phase of valley-fill, comprising a large, meandering channel with exceptionally well-developed point bars (sub-unit 7.3) was, in part, tide- influenced. This implies the late stage onset of estuarine conditions, most probably linked to the Holocene rise of sea-level. This is supported by the immediately overlying Holocene shelf mud layer (Unit 8) which marks the final termination of fluvial–estuarine deposition on the Sunda Shelf.
8. Regional isopach and depth-structure data shows that the valley occupied the axial zone of the Malay Basin. It is located immediately above the deepest part of the basin, where Oligo-Miocene to Pliocene subsidence rates were at their highest, and the NNW–SSE valley trend is parallel the structural contours that define the depth to the top of the basement.
9. The palaeo-Chao Phraya-Johore River is interpreted to be controlled by three different segments: (i) the up-stream segment was controlled by an active mountain belt tectonics and climate. (ii) The mid-stream segment (the study area) was influenced by the lower relief mountains of the Malay Peninsula, which were tectonically inactive. This segment was also characterised by a humid tropical climate and by relatively minor movements along north-west/south-east trending extensional faults, which influenced the orientation of tributaries to the main trunk river. Regional subsidence patterns in the mid-stream segment controlled the NNW–SSE orientation of the main trunk river. (iii) The down-stream segment was mainly controlled by sea-level fluctuations in the South China Sea. In this area, the very low-gradient (*ca* 0.01° dip) and the significant relative fall in sea-level (*ca* 120 m) during

the LGM, resulted in exposure of the whole Sunda Shelf and triggered fluvial incision and valley formation.

## **ACKNOWLEDGMENTS**

This research was completed and supported by a scholarship to the first author from King Abdulaziz University, Saudi Arabia. PETRONAS is also gratefully acknowledged for providing 3D seismic and site survey data and for approving the publication of this paper. We would especially like to thank: Khairul Sulaiman, Nor Azhar Ibrahim, Rais and Deva Ghosh for helpful discussions about the fluvial systems of Miocene to Recent successions of the Malay Basin. Special thanks go to Gary Hampson for reading an earlier version of the research and for making many helpful suggestions. We would also like to thank Exprodat, especially Alex Davis, Chris Jepps and Gareth Smith, for their help in using ArcGIS and developing a semi-automated methodology to quantify the channel morphometric parameters.

## **REFERENCES**

- Allen, J.R.L.** (1965) Late Quaternary Niger delta, and adjacent areas: sedimentary environments and lithofacies. *AAPG Bull.*, **49**, 547-600.
- Allen, G.P.** and **Chambers, J.L.C.** (1998) *Sedimentation in the Modern and Miocene Mahakam Delta*. Indonesia Petroleum Association, 236 pp.
- Alqahtani, F.A.** (2010) *3D seismic geomorphology of fluvial systems*. PhD. thesis, Imperial College London, 251 pp.

**Arshad, A.M., Dashuki, M. and Tjia, H. D.** (1995) A deep seismic section across the Malay Basin; processing of data and tectonic interpretation. *Bull. Geol. Soc. Malaysia*, **21**, 412.

**Bard, E., Hamelin, B. and Fairbanks, R.G.** (1990) U-Th obtained by mass spectrometry in corals from Barbados: sea level during the past 130,000 years. *Nature*, **346**, 456–458.

**Best, J.L. and Ashworth, P.J.** (1997) Scour in large braided rivers and the recognition of sequence stratigraphic boundaries. *Nature*, **387**, 275–277.

**Blum, M.D.** (1994) Genesis and architecture of incised valley fill sequences: a late Quaternary example from the Colorado River, gulf coastal plain of Texas. In: *Siliciclastic Sequence Stratigraphy: Recent Developments and Applications* (Eds. P. Weimer & H.W. Posamentier). *AAPG Memoir*, **58**, 259-283.

**Blum, M.D. and Törnqvist, T.E.** (2000) Fluvial responses to climate and sea level change: a review and look forward. *Sedimentology*, **47**, 2–48.

**Bridge, J.S.** (2003) *Rivers and Floodplains; Forms, Processes, and Sedimentary Record*. Blackwell Publishing, Oxford, 504 pp.

**Brown, A.R.** (2004) *Interpretation of three-dimensional seismic data, 6<sup>th</sup> edition*. *AAPG Memoir 42*. Tulsa, Oklahoma, 541 pp.

**Carlston, C.W.** (1965) The relation of free meander geometry to stream discharge and its geomorphic implications. *American J. Sci.*, **263**, 864–885.

This article is protected by copyright. All rights reserved.

**Chappell, J., Omura, A., Esat, T., Mcculloch, M., Pandol, J., Ota, Y. and Pillans, B.** (1996) Reconciliation of late Quaternary sea levels derived from coral terraces at Huon Peninsula with deep-sea oxygen isotope records. *Earth Planet. Sci. Lett.*, **141**, 227-236.

**Clift, P.D.** (2006) Controls on erosion of Cenozoic Asia and the flux of the clastic sediment to the ocean. *Earth Planet. Sci. Lett.*, **241**, 571-580.

**Clift, P.D. and Plumb, R.A.** (2008) *The Asian Monsoon: Causes, History and Effects*. Cambridge University Press, 288 pp.

**Coleman, J.M., Gagliano, S.M., and Smith, W.G.** (1970) Sedimentation in a Malaysian high tide delta. In: *Deltaic Sedimentation, Modern and Ancient* (Eds J.P. Morgan). *Soc. Econ. Paleontol. and Mineral., Spec. Publ.*, **15**, 185-197.

**Collins, D.S., Allison, P.A. Johnson, H.D., Avdis, A., Hill, J. and Piggott, M.** (2014) Integrating tidal modelling and facies analysis for the Miocene, Northwest Borneo, South China Sea. *AAPG Search and Discovery Article*, 50990.

**Dalrymple, R.W., Zaitlin, B.A. and Boyd, R.** (1992) Estuarine facies models: conceptual basis and stratigraphic implications. *J. Sedim. Petrol.*, **62**, 1130-1146.

**Dalrymple, R.W., Boyd, R., and Zaitlin, B.A.** (Eds) (1994) *Incised Valley Systems: Origin and Sedimentary Sequences*. SEPM Spec. Publ., **51**, 391 pp.

**Dalrymple, R.W., Leckie, D.A., and Tillman, R.W.** (Eds) (2006) *Incised Valleys in Time and Space*. SEPM Spec. Publ., **85**, 343 pp.

This article is protected by copyright. All rights reserved.

**Dalrymple, R.W., Zaitlin, B.A. and Boyd, R.** (1992) Estuarine facies models: conceptual basis and stratigraphic implications. *J. Sed. Petrol.*, **62**, 1130–1146.

**Darmadi, Y., Willis, B.J. and Dorobek, S.L.** (2007) Three-dimensional seismic architecture of fluvial sequences on the low gradient Sunda Shelf, offshore Indonesia. *J. Sed. Research*, **77**, 225-238.

**Davidson, S.K. and North, C.P.** (2009) Geomorphological regional curves for prediction of drainage area and screening modern analogues for rivers in the rock record. *J. Sed. Res.*, **79**, 773–792.

**Dury, G.H.** (1976) Change prediction, present and former, from channel dimensions. *J. of Hydrology*, **30**, 219–245.

**Emery, D. and Myers, K.J.** (Eds) (1996) *Sequence Stratigraphy*. Blackwell Science, Oxford, 297 pp.

**Fielding, C.R. and Gibling, M.R.** (2005) Distinguishing between channel and valley fills: definitions, diagnostic criteria and dimensional data. *8th International Conference on Fluvial Sedimentology*. Delft, Netherlands, Abstracts, 101 pp.

**Fisk, H.N. and Mcfarlan Jr. E.** (1955) Late Quaternary deltaic deposits of the Mississippi River. *Geol. Soc. of America, Special Paper*, **62**, 279–302.

**Gascoyne, M., Benjamin, G.J. and SCWARTZ, H.P.** (1979) Sea-level lowering during the Illinoian glaciations: evidence from a Bahama “Blue Hole”. *Science* **205**, 806-808.

This article is protected by copyright. All rights reserved.

**Ghosh, D., Firdaus Abdul Halim, M., Brewer, M., Viratno, B. and Darman, N.** (2010) Geophysical issues and challenges in Malay and adjacent basins from an E & P perspective. *The Leading Edge*, 436-449.

**Gibling, M.R.** (2006) Width and thickness of fluvial channel bodies and valley fills in the geological record: a literature compilation and classification: *J. Sed. Research*, **76**, 731-770.

**Green, A.N.** (2009) Palaeo-drainage, incised valley fills and transgressive systems tract sedimentation of the northern KwaZulu-Natal continental shelf, South Africa, SW Indian Ocean. *Marine Geology*. **263**, 46-63.

**Hamilton, W.** (1979) *Tectonics of the Indonesian region*. US Geol. Survey Professional Paper, 345 pp.

**Hampson, G.J., Elliot, T. and Davies, J.** (1997) The application of sequence stratigraphy to Upper Carboniferous fluvio-deltaic strata of the onshore UK and Ireland: implications for the southern North Sea. *J. Geol. Soc. Lond.*, **154**, 719-733.

**Hanebuth, T.J., Statteger, K. and Grootes, P.M.** (2000) Rapid Flooding of the Sunda Shelf: A Late-Glacial Sea-level Record. *Science*, **288**, 1033-1035.

**Hanebuth, T.J. and Statteger, K.** (2003) The stratigraphic evolution of the Sunda Shelf during the past fifty thousand years. In: *Tropical deltas of Southeast Asia: Sedimentology, Stratigraphy, and Petroleum Geology* (Eds H.F. Sidi, D. Nummedal, P. Imbert and H. Darman), *SEPM Spec. Publ.*, **76**, 189-200.

This article is protected by copyright. All rights reserved.

**Hanebuth, T.J., Statterger, K., Schimanski, A., Lüdmann, T. and Wong, H.K.** (2003) Late Pleistocene forced regressive deposits on the Sunda Shelf (SE Asia). *Marine Geology*, **199**, 139-157.

**Hanebuth, T.J., Voris, H.K., Yokoyama, Y., Saito, Y. and Okuno, J.** (2011) Formation and fate of sedimentary depocentres on Southeast Asia's Sunda Shelf over the past sea-level cycle and biogeographic implications. *Earth-Science Reviews*, **104**, 92-110.

**Hiscott, R.N.** (2003) Latest Quaternary Baram Prodelta, Northwestern Borneo. In: *Tropical deltas of Southeast Asia: sedimentology, stratigraphy, and petroleum geology* (Eds H.F. Sidi, D. Nummedal, P. Imbert and H. Darman), *SEPM Spec. Publ.*, **76**, 89-107.

**Hopkins, D.M.** (1982) Aspects of the paleoecology of Beringia during the Late Pleistocene. In: *Paleoecology of Beringia* (Eds D. M. Hopkins, J. V. Matthews, C. E. Schweger and S. B. Young), *Academic Press*, New York, 3-28.

**Hutchison, C.S.** (1989) *Geological Evolution of South East Asia*. Oxford monographs on Geology and Geophysics **13**, 368 pp.

**Huffman, O.F.** (1999) Variety in the Paleoenvironment of Early Homo erectus of Java, Indonesia. *J. Human Evolution*, **36**, A8-A9,

**Huffman, O.F.** (2001) Plio-Pleistocene environmental variety in eastern Java and early Homo erectus paleoecology - a geological perspective. In: T. Simanjuntak, B. Prasetyo & R. Handini (eds.), *Sangiran: Man, Culture, and Environment*. In: *Pleistocene Times*,



*Proceedings of the International Colloquium on Sangiran Solo - Indonesia*, Jakarta, 231-256.

**Huffman, O.F.** and **Zaim, Y.** (2003) Mojokerto Delta, East Jawa: Paleoenvironment of *Homo modjokertensis*-First Results. *J. Mineral Technology*, **10**, 1-32.

**Isa, Z.M., Richard, F.W.** and **Yunus, H.** (1992) Integration of 3D and site survey seismic data in analysis of near-surface hazards to platform location at Dulang field. Malay Basin: *Geol. Soc. Malaysia Bulletin*, **32**, 165-184.

**Jones, B.G., Woodroffe, C.D.** and **Martin, G.R.** (2003) Deltas in the Gulf of Carpentaria, Australia: Forms, Processes, and Products. In: *Tropical deltas of Southeast Asia: Sedimentology, Stratigraphy, and Petroleum Geology* (Eds H.F. Sidi, D. Nummedal, P. Imbert and H. Darman), *SEPM Spec. Publ.*, **76**, 21-43.

**Kiel, B.A.** and **Wood, L.J.** (2011) Three-dimensionality, longitudinal profile setting, and paleo-discharge capacity of incised valleys in recent stratigraphy of the Sunda Shelf, Indonesia. *Zeitschrift fur Geomorphology*, **55**, 475-491.

**Kiel, B.A.** and **Wood, L.J.** (2012) Seismic attributes correlated with incised valley thickness in recent stratigraphy of the Sunda Shelf, Indonesia. *Zeitschrift fur Geomorphology*, **56**, 1-18.

**Kuehl, S.A., Allison, M.A., Goodbred, S.L.** and **Kudrass, H.** (2005) The Ganges-Brahmaputra Delta. In: *River Deltas - Concepts, Models, and Examples* (Eds L. Giosan and J.P. Bhattacharya). *SEPM Spec. Publ.*, **83**, 413-434.

**Loe, C.T.** (1997) Exploration in the Gulf of Thailand in deltaic reservoirs, related to the Bangkok Field. In: *Petroleum Geology of Southeast Asia* (Eds A.J. Fraser, S.J. Matthews and R.W. Murphy), *Geol. Soc. Spec. Publ.*, **126**, 77-87.

**Leopold, L.B.** and **Wolman, M.G.** (1957) River Channel patterns: braided, meandering and straight. *Geological Survey Professional Paper*, **282-B**, 49 pp.

**Mackey, S.D.** (1993) *Theoretical modeling of alluvial architecture*. PhD thesis, State University of New York, 421 pp.

**Madon, M.B.** (1999) Basin types, tectono-stratigraphic provinces, structural styles. In: *The Petroleum Geology and Resources of Malaysia* (Eds PETRONAS), 77-111.

**Madon, M.B., Abolins, P., Jamaal Hoesni, M.** and **Bin Ahmad, M.** (1999) Malay Basin, In: *The Petroleum Geology and Resources of Malaysia* (Eds PETRONAS) 173-217.

**Madon, M.B.** and **Watts, A.B.** (1998) Gravity anomalies, subsidence history and the tectonic evolution of the Malay and Penyu basins (offshore Peninsula Malaysia). *Basin Research*, **10**, 375-392.

**Marriott, S.B.** (1999) The use of models in the interpretation of the effects of base-level change on alluvial architecture. In: *Fluvial Sedimentology VI, Proceedings* (Eds N.D. Smith and J. Rogers), *Spec. Public. Int. Ass. Sed.*, **28**, 271-281.

**Martin, J., Cantelli, A., Paola, C., Blum, M.** and **Wolinsky, M.** (2011) Quantitative modelling of the evolution and geometry of incised valleys. *J. Sedi. Res.*, **81**, 64-79.

**Mattheus, C.R. and Rodriguez, A.B.** (2011) Controls on late Quaternary incised-valley dimension along passive margins evaluated using empirical data. *J. Sed. Res.*, **77**, 213–224.

**Mattheus, C.R., Rodriguez, A.B., Greene, D.L., JR, Simms, A.R. and Anderson, J.B.** (2007) Control of upstream variables on incised-valley dimension. *Sedimentology*, **58**, 1113–1137.

**Mertes, L., and Dunne, T.** (2007) The effects of tectonism, climate change, and sea-level change on the form and behaviour of the modern Amazon River and its floodplain. In *Large Rivers* (Eda A. Gupta), 115-144..

**Me´tivier, F., Gaudemer, Y., Tapponnier, P. and Klein, M.** (1999) Mass accumulation rates in Asia during the Cenozoic. *J. Geophys. Int.*, **137**, 280–318.

**Miall, A.D.** (1996) *The Geology of Fluvial Deposits*. Springer-Verlag, New York, 582 pp.

**Miall, A.D.** (2002) Architecture and sequence stratigraphy of Pleistocene fluvial systems in the Malay Basin, based on seismic time slices analysis. *AAPG Bulletin*, **86**, 1201–216.

**Milliman, J.D., Farnsworth, K.L., and Albertin, C.S.** (1999) Flux and fate of fluvial sediments leaving large islands in the East Indies. *J. of Sea Research*, **41**, 97-107.

**Mitchum, R.M., Vail, P.R. and Thompson, S. III.** (1977) Seismic stratigraphy and global changes of sea-level part 2: the depositional sequence as a basic unit for stratigraphic

analysis. In: *Seismic Stratigraphy – Applications to Hydrocarbon Exploration* (Eds C.E. Paynton). *AAPG Memoir*, **26**, 53-62.

**Molengraaff, G.F. and Weber, M.** (1921) On the relation between the Pleistocene glacial period and the origin of the Sunda Sea (Java- and South China Sea), and its influence on the distribution of coral reefs and on the land- and freshwater fauna. *Proceedings Royal Academy*, **23**, 395–439.

**Morley, R.J.** (2000) *Origin and Evolution of Tropical Rain Forests*. John Wiley & Sons, Chichester, 378 pp.

**Morley, C.K. and Westaway, R.** (2006) Subsidence in the super-deep Pattani and Malay basins of Southeast Asia: A coupled model incorporating lower-crustal flow in response to post-rift sediment loading. *Basin Research*, **18**, 51–84.

**Morley, C.K. and Racey, A.** (2011) *Tertiary stratigraphy*. In: *The Geology of Thailand*. (Eds M. F., Ridd, A. J., Barber, and M. J., Crow,) *Geol. Soc. Lond.*, 223-271.

**Morley, C.K., Charusiri, P. and Watkinson, I.M.** (2011) Structural geology of Thailand during the Cenozoic In: *The Geology of Thailand*. (Eds M. F., Ridd, A. J., Barber, and M. J., Crow) *Geol. Soc. Lond.*, 273-334.

**Ngah, K., Madon, M.B. and Tjia, H.D.** (1996) Role of pre-Tertiary fractures in formation and development of the Malay and Penyu basins. In: *Tectonic Evolution of Southeast Asia* (Eds R. Hall & D.J. Blundell), *Geol. Soc. Lond. Spec. Publ.*, **106**, 281-289.

**Nordfjord, S., Goff, J.A., Austin, J.A.J. and Gulick, S.P.S.** (2006) Seismic facies of incised-valley fills, New Jersey continental shelf: implications for erosion and preservation processes acting during latest Pleistocene–Holocene transgression. *J. Sed. Research*, **76**, 1284–1303.

**Nummedal, D., Sidi, F.H. and Posamentier, H.W.** (2003) A framework for deltas in Southeast Asia. In: *Tropical deltas of Southeast Asia: Sedimentology, Stratigraphy, and Petroleum Geology* (Eds H.F. Sidi, D. Nummedal, P. Imbert and H. Darman), *SEPM Spec. Publ.*, **76**, 5-17.

**Oomkens, E.** (1974) Lithofacies relations in the Late Quaternary Niger delta complex. *Sedimentology*, **21**, 195-222.

**Osterkamp, W.R. and Hedman, E.R.** (1982) Perennial streamflow characteristics related to channel geometry and sediment in Missouri River basin; *USGS Prof. Paper.*, **1242**, 847–851.

**Paquet, F., Menier, D., Estournès, G., Bourillette, J.F., Leroy, P. and Guillocheau, F.** (2010) Buried fluvial incisions as a record of Middle-Late Miocene eustasy fall on the Armorican Shelf (Bay of Biscay, France). *Marine Geology*, **268**, 137-151.

**Posamentier, H.W.** (2000) Seismic stratigraphy into the next millennium: a focus on 3D seismic data. *AAPG Annual Conference*, New Orleans, Louisiana, 16-19.

**Posamentier, H.W.** (2001) Lowstand alluvial bypass systems: incised vs. Unincised. *AAPG Bulletin*, **85**, 1771–1793.

**Posamentier, H.W., Allen, H.W., James, D.P. and Tesson, M.** (1992) Forced regressions in a sequence stratigraphic framework: Concepts, examples, and sequence stratigraphic significance. *AAPG Bulletin*, **76**, 1687-1709.

**Posamentier, H.W. and Allen, G.P.** (1999) *Siliciclastic Sequence Stratigraphy—Concepts and Applications: concepts in Sedimentology and Paleontology*. *SEPM Spec. Publ.*, **7**, 210 pp.

**Posamentier, H.W., Davies, R.J., Wood, L.J. and CARTWRIGHT, J.A.** (2007) Seismic geomorphology-an overview. In: *Seismic Geomorphology* (Eds R.J. Davies, H.W. Posamentier, L.J. Wood and J.A. Cartwright), *Geol. Soc. Lond Spec. Publ.*, **27**, 1-14.

**Posamentier, H.W., Jervey, M.T. and Vail, P.R.** (1988) Eustatic controls on clastic deposition I-conceptual framework. In: *Sea-Level Changes: An Integrated Approach* (Eds C.K. Wilgus), *SEPM Spec. Publ.*, **42**, 109–124.

**Pubellier, M. and Morley, C.K.** (2014) The Basins of Sundaland (SE Asia); evolution and boundary conditions. *Marine and Petroleum Geology* (in press).

**Reijnenstein, H.M., Posamentier, H.W. and Bhattacharya, J.P.** (2011) Seismic geomorphology and high-resolution seismic stratigraphy of inner-shelf fluvial, estuarine, deltaic, and marine sequences, Gulf of Thailand. *AAPG Bulletin*, **95**, 1959–1990.

**Razak, Z., Zuhairi, A., Shahbudin, S. and Rosnan, Y.** (2012) 2-Dimensional Hydrodynamic Patterns of Pahang River Estuary, Pahang, Malaysia during Northeast and Southwest Monsoon. *UMT 11th International Annual Symposium on Sustainability Science and Management, Terengganu, Malaysia*, 1357-1371.

This article is protected by copyright. All rights reserved.

**Reijnenstein, H.M., Posamentier, H.W. and Bhattacharya, J.P.** (2011) Seismic geomorphology and high-resolution seismic stratigraphy of inner-shelf fluvial, estuarine, deltaic, and marine sequences, Gulf of Thailand. *AAPG Bulletin*, **95**, 1959–1990.

**Reynaud, J., Tessier, B., Proust, J., Dalrymple, R., Bourillet, J., De Batistatist, M., Lericolais, G., Berné, S., and Marsett, T.** (1999) Architecture and sequence stratigraphy of a late Neogene incised valley at the shelf margin, southern Celtic Sea. *J. of Sed. Research*, **69**, 351 pp.

**Sandal, S.T.** (1996) *The Geology and Hydrocarbon Resources of Negara Brunei Darussalam*. Brunei Shell Petroleum Sendiran Berhad & Brunei Museum, 243 pp.

**Sathiamurthy, E. and Voris, H.K.** (2006) Maps of Holocene sea level transgression and submerged lakes on the Sunda Shelf. *The Natural History Journal of Chulalongkorn University, Supplement*, **2**, 1-44.

**Schumm, S.A.** (1993) River response to baselevel change: implications for sequence stratigraphy. *J. Geol.*, **101**, 279–294.

**Schumm, S.A.** (2005) *River Variability and Complexity*. Cambridge University Press, Cambridge, 234 pp.

**Schumm, S.A. and Ethridge, F.G.** (1994) Origin, evolution and morphology of fluvial valleys. In: *Incised-Valley Systems: Origin and Sedimentary Sequences* (Eds R.W. Dalrymple, B.A. Zaitlin & P.A. Scholle), *SEPM Spec. Publ.*, **51**, 11–27.

**Shackleton, N.J.** (1987) Oxygen isotopes, ice volume and sea level. *Quaternary Science Reviews*, **6**, 183-190.

**Shanley, K.W.** and **McCabe, P.J.** (1993) Alluvial architecture in a sequence stratigraphic framework; a case history from the Upper Cretaceous of southern Utah, USA. In: *The Geological Modelling of Hydrocarbon Reservoirs and Outcrop Analogues* (Eds S.S. Flint & A.D. Bryant), *Int. Assoc. Sed. Spec. Publ.*, **15**, 21-55.

**Shanley, K.W.** and **McCabe, P.J.** (1994) Perspectives on the sequence stratigraphy of continental strata. *AAPG Bulletin*, **78**, 544-568.

**Sidi, F.H., Nummedal, D. Imbert, P.** and **Darman, H.** (Eds) (2003) *Tropical deltas of Southeast Asia: Sedimentology, Stratigraphy, and Petroleum Geology*. *SEPM Spec. Publ.*, **76**, 269 pp.

**Sinsakul, S.** (1992) Evidence of quaternary sea level changes in the coastal areas of Thailand. *J. Southeast Asian Earth Sci.*, **7**, 23-37.

**Staub, J.R.** and **Gastaldo, R.A.** (2003) Late Quaternary sedimentation and peat development in the Rajang River Delta, Sarawak, east Malaysia In: *Tropical deltas of Southeast Asia: Sedimentology, Stratigraphy, and Petroleum Geology* (Eds H.F. Sidi, D. Nummedal, P. Imbert & H. Darman), *SEPM Spec. Publ.*, **76**, 71-87.

**Staub, J.R., Among, H.L.** and **Gastaldo, R.A.** (2000) Seasonal sediment transport and deposition in the Rajang River delta, Sarawak, East Malaysia. *Sedimentary Geology*, **133**, 249-264.



**Strong, N.** and **Paola, C.** (2006) Fluvial landscapes and stratigraphy in a flume. *The Sedimentary Record*, **4**, 4-7.

**Sümeğhy, B.**, and **Kiss, T.** (2011) Discharge calculation of the paleochannels on the alluvial fan of the Maros River, Hungary. *J. of Environmental Geography*, **4**, 11-17.

**Sun, X.**, **Li, X.**, **Luo, Y.** and **Chen, X.** (2000) The vegetation and climate at the last glaciation on the emerged continental shelf of the South China Sea. *Palaeogeography, Palaeoclimatology, Palaeoecology*, **160**, 301-316.

**Ta, T.K.O.**, **Nguyen, V.L.**, **Tateishi, M.**, **Kobayashi, I.**, **Tanabe, S.** and **Saito, Y.** (2002) Holocene delta evolution and sediment discharge of the Mekong River, southern Vietnam. *Quaternary Science Reviews*, **21**, 1807-1819.

**Ta, T.K.O.**, **Nguyen, V.L.**, **Tateishi, M.**, **Konayashi, I.** and **Saito, Y.** (2005) Holocene delta evolution and depositional models of the Mekong River Delta, southern Vietnam. In: *River Deltas – Concepts, Models and Examples* (Eds L. Giosan and J. P. Bhattacharya). SEPM Spec. Publ., **83**, 453-466.

**Talling, P.J.** (1998) How and where do incised valleys form if se level remains above the shelf edge? *Geology*, **26**, 87-90.

**Tamura, T.**, **Saito, Y.**, **Sieng, S.**, **Ben, B.**, **Kong, M.**, **Sim, I.**, **Choup, S.** and **Akiba, F.** (2009) Initiation of the Mekong River delta at 8 ka: evidence from the sedimentary succession in the Cambodian lowland. *Quaternary Science Reviews*, **28**, 327-344.

**Tanabe, S., Ta, T.K.O., Nguyen, V.L., Tateishi, M., Kobayashi, I. and Saito, Y.** (2003) Delta evolution model inferred from the Holocene Mekong Delta, southern Vietnam. In: *Tropical deltas of Southeast Asia: sedimentology, stratigraphy, and petroleum geology* (Eds H.F. Sidi, D. Nummedal, P. Imbert & H. Darman), *SEPM Spec. Publ.*, **76**, 175-188.

**Tapponnier, P., Pltzer, G. and Armijo, R.** (1986) On the mechanics of the collision between India and Asia. In: *Collision tectonics* (Eds M.P. Coward & A.C. Ries), *Geol. Soc. Spec. Publ.*, **19**, 115-157

**Tjia, H.D.** (1980) The Sunda shelf, Southeast Asia. *Annals of Geomorphology*, **4**, 405-427.

**Tjia, H.D.** (1994) Inversion tectonics in the Malay Basin: evidence and timing of events. *Geol. Soc. Malaysia Bulletin*, **36**, 119-126.

**Tjia, H.D. and Liew, K.K.** (1996) Changes in tectonic stress field in northern Sunda Shelf basins. In: *Tectonic Evolution of Southeast Asia* (Eds R. Hall & D.J. Blundell), *Geol. Soc. Lond. Spec. Publ.*, **106**, 291-306.

**Thomas, R. G., Smith, D. G., Wood, J. M., Visser, J., Calverley-Range, E. A. and Koster, E. H.** (1987) Inclined Heterolithic Stratification – Terminology, Description and Significance. *Sedimentary Geology*, **53**, 123-179.

**Thorp, M.B., Thomas, M.F., Martin, T. and Whalley, W.B.** (1990) Late Pleistocene sedimentation and landform development in western Kalimantan (Indonesian Borneo). *Geologie en Mijnbouw*, **96**, 133-150.

**Unverricht, D., Szczuciński, W., Stattegger, K., Jagodziński, R.,**

**Xuan Thuyen L. and Wee Kwong, L.** (2013) Modern sedimentation and morphology of the subaqueous Mekong Delta, Southern Vietnam. *Global and Planetary Change*, **110**, 223-235.

**Vail, P.R., Mitchum, R.M. and Thompson, S.III.** (1977) Seismic stratigraphy and global changes of sea level: relative changes of sea level from coastal onlap. In: *Seismic Stratigraphy–Applications to Hydrocarbon Exploration* (Ed. by C.E. Payton) *AAPG Memoir*, **26**, 63-81.

**Van Wagoner, J.C., Posamentier, H.W., Mitchum, R.M., Vail, P.R., Sarg, J.F., Loutit, T.S. and Hardenbol, J.** (1988) An overview of the fundamentals of sequence stratigraphy and key definitions. In: *Sea-Level Changes, An Integrated Approach* (Eds C.K. Wilgus, C.G. Hastings, St. C. Kendall, H.W. Posamentier, C.A. Ross, and J.C. Van Wagoner) Soc. of Econ. Petrol. and Mineral. Spec. Publ., **42**, 39-45.

**Van Wagoner, J.C., Mitchum, R.M., Campion, K.M. and Rahmanian, V.D.** (1990) *Siliciclastic sequence stratigraphy in well logs, cores, and outcrops: concepts for high-resolution correlation of time and facies. AAPG Methods in Exploration Series*, **7**, 55 pp.

**Voris, H.K.** (2000) Maps of Pleistocene sea levels in Southeast Asia: shorelines, river systems and time durations. *Journal of Biogeography*, **27**, 1153-1167.

**Wang, L., Sarnthein, M., Erlenkeuser, H., Grimalt, J., Grootes, P., Heilig, S., Ivanova, E., Kienast, M., Pelejero, C. and Flaumann, U.** (1999) East Asian monsoon climate

during the Late Pleistocene: high-resolution sediment records from the South China Sea. *Marine Geology*, **156**, 245–284.

**Williams, G.P.** (1984) *Developments and applications of geomorphology*, Springer-Verlag Berlin Heidelberg, 372 pp.

**Wong, H.K., Haft, C., Paulsen, A.M., Lu'Dmann, T., Hu"Bscher, C. and Geng, J.** (2003) Late Quaternary sedimentation and sea-level fluctuations on the northern Sunda Shelf, southern South China Sea. In: *Tropical deltas of Southeast Asia: sedimentology, stratigraphy, and petroleum geology* (Eds H.F. Sidi, D. Nummedal, P. Imbert & H. Darman), *SEPM Spec. Publ.*, **76**, 101-127.

**Woodroffe, C.D.** (2000) Deltaic and estuarine environments and their Late Quaternary dynamics on the Sunda and Sahul shelves. *J. Asian Earth Sci.* **18**, 393-413.

**Wright, V.P. and Marriott, S.B.** (1993) The sequence stratigraphy of fluvial depositional systems: the role of floodplain sediment storage. *Sedimentary Geology*, **86**, 203–210.

**Yang, H. and Xie, Z.** (1984) Sea-Level Changes in East China over the Past 20 000 Years. In: *The Evolution of the East Asian Environment* (Eds R.O. Whyte), Univ. Hong Kong, Cent. Asian Stud, 288–308.

**Zaitlin, B.A., Dalrymple, R.W. and Boyd, R.** (1994) The stratigraphic organization of incised-valley systems associated with relative sea-level change. In: *Incised-Valley Systems: Origin and Sedimentary Sequences* (Eds R.W. Dalrymple, B.A. Zaitlin & P.A. Scholle), *SEPM Spec. Publ.*, **51**, 45–60.

**Zeng, H., Backus, M.M., Barrow, K.T. and Tyler, N.** (1998) Stratal slicing; Part 1, Realistic 3-D seismic model: *Geophysics*, **63**, 502-513.

**Zu, T., Gana, J. and Erofeevac, S.Y.** (2008) Numerical study of the tide and tidal dynamics in the South China Sea. *Deep-Sea Research*, **55**, 137-154.

**Zuo Xue, Liu, J.P., DeMaster, D., Van Nguyen, L. and Oanh, T.K.** (2010) Late Holocene Evolution of the Mekong Subaqueous Delta, Southern Vietnam. *Marine Geology*, **269**, 46-60.

#### **FIGURE CAPTIONS**

Fig. 1. Location map of the study area within the Malay Basin (2) on Sunda Shelf, Southeast Asia. The study area is *ca* 700 km away from the present-day shelf break and a few hundred kilometres basinward of the modern shoreline. The blue dashed-lines represent the continental shelf edge (*ca* 200 m bathymetry) and the shallow areas of the Sunda Shelf that were exposed during the sea-level falls. The present-day water depth within the study area ranges from 50 to 80 m. The red dashed-line (A–A') represents the regional cross-section shown in Fig. 3. The blue solid-line represents the equator line. Locations of previous studies of Posamentier (2001), Miall (2002) and Darmadi et al. (2007) are also shown.

Fig. 2. Generalised stratigraphic column of the Malay Basin. The studied interval is the upper part of Group A succession, which is mainly composed of coastal plain deposits (Modified from Madon, 1999).

Fig. 3. Regional south-west/north-east cross-section through the Malay Basin. The main regional stratigraphic intervals are labelled A to M. Location of this cross-section is

shown in Fig. 1. The studied interval lies within the post-inversion Upper Pliocene to Recent interval (modified from Madon, 1999).

Fig. 4. Time-structure map along Horizon (F), showing an area of significant low relief in the central part of the study area (blue colours). The seismic data used in this study consist of ten surveys that have been merged to make a single interpretable volume. The yellow circle represents the location of the well (Tunggal-1) that was used in the time-depth conversion. The white circles represent the locations of the site investigation boreholes used in this study (see Table 1 for more details). The white dashed lines illustrate the locations of the seismic sections shown on Figs 5A and 6 and high-resolution seismic (Boomer data) section shown on Fig. 8, respectively.

Fig. 5. (A) Uninterpreted and (B) interpreted regional seismic section through the 3D seismic dataset illustrating the seismic units (1 to 8) and the bounding surfaces (Horizons A to H). Major channel systems are also shown as 'U' and 'V' shapes. The main bounding surfaces (Horizons A to F) are characterised by prominent incisions. Note the angular discordance between Horizon A and underlying unit at the basin margin (right side of cross-section). The location of this section is shown in Fig. 4. (C) A schematic cross-section through the study area showing the seismic units (1 to 8) and the bounding surfaces (Horizons A to H). Two major incised valleys are shown (in purple), while other large channel systems are shown by either their 'U'-shaped or 'V'-shaped cross-sectional geometries. Smaller high-sinuosity and moderate-sinuosity channels are coloured yellow and dark grey, respectively. Background facies comprise a mud-dominated coastal plain (light grey).

Fig. 6. (A) Uninterpreted and (B) interpreted seismic section through the 3D seismic dataset illustrating the Units 6 to 8 and the sub-units of Unit 7 and the bounding surfaces

(E, F, G and H). (C) A geoseismic interpretation of the same line. Note the different seismic expression within the deep incision compared to that of the adjacent strata. The 'V'-shaped channel morphology associated with lateral accretion surfaces, which is underlain by lenticular bodies, is also shown. Note the stratal truncations at the margins of the deep incision. The location of this section is shown in Fig. 4.

Fig. 7. Two simplified lithological logs, based on site survey borehole data, illustrating the facies characteristics and their calibration with a 3D seismic section: (A) stratigraphy of the abandoned channel-fill, within the incised valley; and (B) stratigraphy of the floodplain outside the incised valley. In (A) the gravels and cobbles with interbedded sands and stiff clay directly overlie a major erosion surface, which defines the base of the incised valley. The highly-sinuuous channel at the top of the incised valley is mainly filled with stiff clay with inclined heterolithic stratification (IHS). These IHS are clearly imaged in the high-resolution seismic section shown on Fig. 8. Thick soft clay (16 m) capped the incised valley and probably represents a layer of Holocene marine mud. In (B) note the absence of pebble-grade and cobble-grade sediment and the dominance of silty clays with shell and plant debris. Together the latter suggest a lower coastal plain depositional environment, with marine to brackish water influence, in the pre-valley-fill succession.

Fig. 8. Uninterpreted (A) and interpreted (B) high-resolution seismic line showing the 'V'-shaped morphology of the highly-sinuuous channel identified at the top of the incised valley. The IHS of the channel fill is clearly imaged. Note the seabed depression, which is believed to have been caused by rising gas plumes at the channel flanks. The location of this section is shown on Fig. 4.

Fig. 9. Two interpretive plan-view maps within Unit 6. (A) The lower part of Unit 6, which is dominated by wide straight and very low-sinuosity channels. The majority of

these channels were flowing mainly south-east, towards the South China Sea. The low-sinuosity channels in the southern part were flowing north-east towards the axial zone of the basin. (B) The upper part of Unit 6, which is dominated by medium-scale, moderate-sinuosity channels without scroll bars. Some parts of the channels in the middle part of the study area were eroded by incised valley in Unit 7. The inset rose diagrams summarise the channel orientations shown on this map.

Fig. 10. (A) Time-slice at 108 twt, and (B) interpreted map-view. These diagrams show a large highly-sinuuous channel, which was flowing to the south-east and confined within a wide and deep incised valley. The youngest channel, located at the top of the valley-fill, is clearly imaged and displays well-developed point bars with brighter amplitudes. Smaller channels, possibly tributaries, are shown at the margins of these incisions. (C) Close-up image showing the tributaries on the margins of the main incised valley. (D) Three-dimensional seismic cube showing the vertical and horizontal seismic expression of the latest meandering channel, with its lateral accretion surface and scroll bars. The 'V'-shaped channel morphology of the abandoned channel is clearly imaged. The locations of panels (C) and (D) are shown on panel (A). The location of Fig. 6 is shown on panel (C).

Fig. 11. Late Pleistocene sea-level curves showing the major fall during the LGM when the sea-level was -120 m below the present-day depths. (A) A sea level curve over the past 140 kyr based on estimates obtained from oxygen isotope (Shackleton, 1987) and coral reef records (Chappell et al., 1996; modified from Hanebuth et al., 2003). (B) A sea level curve over the past 500 kyr based on estimates from oxygen isotope data (Bard et al., 1990, modified from Posamentier, 2001). Note the numerous minor fluctuations in sea-level recorded by these high-resolution data.



Fig. 12. A depositional model of the Late Pleistocene, palaeo-Choa Phraya-Johore incised valley, based on the observations within the Malay Basin. The development of this incised valley is related mainly to variations in sea-level. (A) Incision of the valley during the Last Glacial Maximum (LGM), when sea-level fall was at -120 m and when the Sunda Shelf was widely exposed; (B) deposition of fluvial sands, gravels and cobbles during the initial period of slow sea-level rise; (C) transition from low-sinuosity to high-sinuosity channels during continued sea-level rise, with the latest phase including tidal-influence within an estuarine setting; and (D) complete drowning of the incised valley and coastal plain during the Holocene transgression, resulting in deposition of a Holocene mud blanket. The vertical scale is approximated.

Fig. 13. (A) Time slice at 108 ms twt showing a large meandering channel with very well-developed scroll bars; (B) a satellite image of a portion of the Purus River, which is one of the main tributaries of the Amazon. This river has similar geometric characteristics to those observed in the time-slice at 108 twt (in A), namely: width of 500 to 750, depth of 10 to 15 m, meander belt width of 14 to 24 km, and *SI* of 2.8. Note the tributaries at the valley margins in both images.

Fig. 14. A schematic map of the possible drainage basin of the incised valley showing the upstream to downstream reaches of the valley. It shows the correlation of the Unit 7 incised valley, here termed the Johore River, with its inferred upstream equivalent, the Chao Phraya River. The whole drainage area is herein referred to as the palaeo-Choa Phraya-Johore River System. The blue box defines the study area.

Fig. 15. (A) A digital elevation map of Southeast Asia, showing the location of the major rivers: (1) Indus; (2) Ganges; (3) Brahmaputra; (4) Irrawaddy; (5) Choa Phraya; (6) Mekong; (7) Red; (8) Pahang; (9) Rajang; (10) Baram; (11) Barito; (12) Mahakam; and

(13) the studied valley system (palaeo-Choa Phraya-Johore River). (B) Comparison of the size, shape and orientation of the drainage basins of these major river systems.

Fig. 16. Incised valley cross-sectional areas plotted against the drainage basin sizes of the Unit 7 incised valley and those incised valleys that drained to the Gulf of Mexico (data from Mattheus et al. 2007 and Nordfjord et al., 2005).

Fig. 17. (A) Time-slice at 108 twt showing the merged 3D seismic dataset across a larger part of the Malay Basin. The two blue lines represent the valley margins that bound the large meandering channel observed in this study (Fig. 10A). (B) the south-eastwards continuation of the large meandering channel and the change into a straighter channel form, which takes place in a seawards direction (towards the South China Sea) (Fig. 14C). The locations of panels (B) and (C) are shown on panel (A).

Fig. 18. (A) A map showing the palaeo-drainage systems that are still detectable on the modern sea floor (edited from Molengraaff, 1921; Taji, 1980; Voris, 2000). The black box represents the location of panels (B) and (C). (B) Close-up map showing the present-day topographic map of the Sunda Shelf (Sathiamurthy & Voris, 2006), with superimposed pre-Tertiary depth contours (Madon, 1999b). The black solid-lines represent the 'trunk' river described by Voris (2000). The white solid-line represents the youngest channel system observed within the Late Pleistocene river systems; (C) an edited version showing the exact location of the 'trunk' river. This channel was the major channel that occupied the axial zone of the Malay Basin during the Late Pleistocene.

## TABLES

Table 1. Summary of the platform site investigation boreholes analysed in this study.

Table 2. Summary of the main seismic stratigraphic units analysed in this study (from bottom to top, units 6, 7 and 8), their seismic stratigraphic reflection surfaces (D, E and F) and their thickness and channel form properties. The basic information data comprises isochron range and average (in milli-seconds twt), average thickness (m) and the following channel properties: channel width (*CW*), channel depth (*CD*) and sinuosity (*SI*). Channel parameters refer to single channel forms, whereas the incised valley data refers to composite valley-fill form.

Table 3. Summary of the sub-units identified within Unit 7 (from bottom to top: 7.1, 7.2 and 7.3): isochron range (milli-seconds twt), average thickness (m) and the following channel parameters: channel width (*CW*), channel depth (*CD*) and sinuosity (*SI*).

Table 4. Summary of some of the world's largest rivers, plus a selection of those from Southeast Asia, in terms of the following parameters: width (*CW*), meander belt width (*MBW*), depth (*CD*), drainage basin areas and water discharge. These data are compared to the equivalent parameters estimated for the palaeo-Choa Phraya River (in bold).

Table 5. Palaeohydrological estimations of bankfull discharge and average discharge used in this study are based on the methodologies and formulae published by the authors listed in this table. The data listed against the high channel form, all refer to the single, large meandering channel at the top of the incised valley (Unit 7.3) and include the following average input parameters: *ML* = meander length = 14 000 m; *CW* = channel width = 600 m; *S* = slope = 0.0001 degrees.

Table 6. The morphometric parameters of the eastern Gulf of Mexico and New Jersey incised valley systems (data obtained from Mattheus et al., 2007 and Nordford et al., 2005, respectively) compared with data measured in this study for the palaeo-Chao Praya-Johore River. These data were used in the plots of Fig. 13. The following abbreviations are used:  $Vw$  = valley width (maximum);  $Vd$  = Valley depth (maximum) and  $A$  = valley cross-sectional area (average).

**Table 1**

No.	Borehole name	Total depth (m)	Field	Water depth at well location (m)	Location
1	Melor	150.0	Melor Field	76.3	Within IVF
2	Tangga Barat-1A	150.0	Tangga Field	70.9	Within IVF
3	Tangga Barat-1B	150.0	Tangga Field	70.8	Within IVF
4	BH Tangga	150.0	Tangga Field	65.3	Outside IVF
5	Tangga Deep-1	30.0	Tangga Field	63.3	Outside IVF
6	Bujang Deep-1	30.0	Bujang Field	66.1	Outside IVF
7	Dulang A-Primary	150.6	Dulang Field	74.5	Within IVF
8	Dulang A-Secondary	151.6	Dulang Field	74.7	Within IVF
9	Dulang B	150.3	Dulang Field	79.0	Within IVF
10	Dulang WP-B	60.0	Dulang Field	78.4	Within IVF
11	Dulang WP-C	60.0	Dulang Field	75.7	Within IVF
12	Dulang WP-D	60.0	Dulang Field	74.6	Within IVF
13	Dulang SPM-1	30.0	Dulang Field	74.6	Within IVF
14	Dulang SPM-2	45.0	Dulang Field	77.2	Within IVF

---

<b>15</b>	Dulang SPM-3	45.0	Dulang Field	75.6	Within IVF
<b>16</b>	Dulang SPM-C	45.6	Dulang Field	77.3	Within IVF

---

**Table 2**

Unit No.	Base horizon	Top horizon	Thickness range (ms twt)	Average thickness (ms twt)	Average thickness (m)	Channel parameters				Incised valley parameters		
						Stratigraphic level SI	CW (m)	CD (m)	Width (m) SI	Depth (m) SI		
8	F	G	100-82	18	16	-----	-----			-----	----	----
7	E	F	192-100	92	87	Inside IVF	600	25	3	13000-	55-	1.2
						Outside IVF	320-600	15-32	1.1-1.5	-----	----	----
6	D	E	228-108	120	112	U	75-320	8-20	1.3-1.5	-----	----	----
						L	300-1300	15-30	1.0-1.3	-----	----	----

**Table 3**

Sub-unit No.	Average thickness (ms twt)	Average thickness (m)	Seismic facies character	Channel parameters		
				CW (m)	CD (m)	SI
7.3	25-32	23-30	Type-2 channel morphology associated with dipping surfaces	600	25	3
7.2	22-30	20-28	Laterally-continuous reflections with no observed channel morphology	-----	-----	-----
7.1	12-15	10-13	Lenticular, discontinuous seismic facies	-----	-----	-----

**Table 4**

Name	Channel width (m)	Meander belt width (m)	Channel depth (m)	Drainage area (10 <sup>3</sup> km <sup>2</sup> )	Average discharge (m <sup>3</sup> /s)
Amazon	3600	20000	35	6,915	219,000
Congo	1200	8000	20	3,680	41,800
Nile	600	12000	12	3,349	5,100
Mississippi	2500	11000	12	2,980	16,200
Yenisey	3000	17000	24	2,580	19,600
Yangtze	500	6000	11	1,800	31,900
Brahmaputra	1300	13000	25	1,730	19,200
Palaeo Chao Pahraya	<b>600</b>	<b>13500</b>	<b>25</b>	<b>1,350</b>	<b>36,740</b>
Orinoco	2500	10000	26	1,330	34,880
Indus	1500	13000	25	960	7,160
Ganges	1000	8000	21	907	12,037
Mekong	1300	4500	22	810	16,000



<b>Irrawaddy</b>	1300	1100	18	411	13,000
<b>Salween</b>	230	2600	12	324	4,876
<b>Red River</b>	1100	8000	20	143	13,500
<b>Chao Pahraya</b>	250	2400	12	121	3,500
<b>Mahakam</b>	470	6700	12	75	3,300
<b>Rajang</b>	550	4000	13	41	6,000
<b>Pahang</b>	330	3700	10	29	1,712
<b>Barito</b>	400	3800	11	25	7,000
<b>Baram</b>	360	3500	8	10	1,724

**Table 5**

<b>Channel Form</b>		<b>Equation</b>	<b>Author</b>	<b>Bankfull Discharge (Q<sub>b</sub> m<sup>3</sup>/s)</b>	<b>Average Discharge (Q m<sup>3</sup>/s)</b>
<b>High-sinuosity</b>	<b>Planform geometry</b>	$ML = 65.2Q_b^{0.5}$	Leopold & Wolman (1957)	<b>46106</b>	-
		$Q = 0.000017 ML^{2.15}$	Carlston (1965)	-	<b>13952</b>
		$ML = 65.2Q_b^{0.5}$	Mackey (1993)	<b>46550</b>	-
		$Q_b = 0.0003ML^2 + 0.3440ML - 81.329$	Sümeğhy & Kiss (2011)	<b>63535</b>	-
		$Q = 0.027 CW_b^{1.69}$	Osterkamp &	-	<b>1338</b>

			Hedman (1982)		
		$Q_b = 9.93 A_b^{0.85}$	Dury (1976)	<b>35207</b>	-
	<b>Cross-sectional area</b>	$Q_b = 4.0 A_b^{1.21} S^{0.28}$	Williams (1978)	<b>31144</b>	-
<b>Low-sinuosity/Aggradational channel</b>	<b>Cross-sectional area</b>	$Q = (CW*CD)^{5/3} S^{1/2}$ (1.49/n)	Grauckler-Manning	<b>36740</b> for meandering channel	-

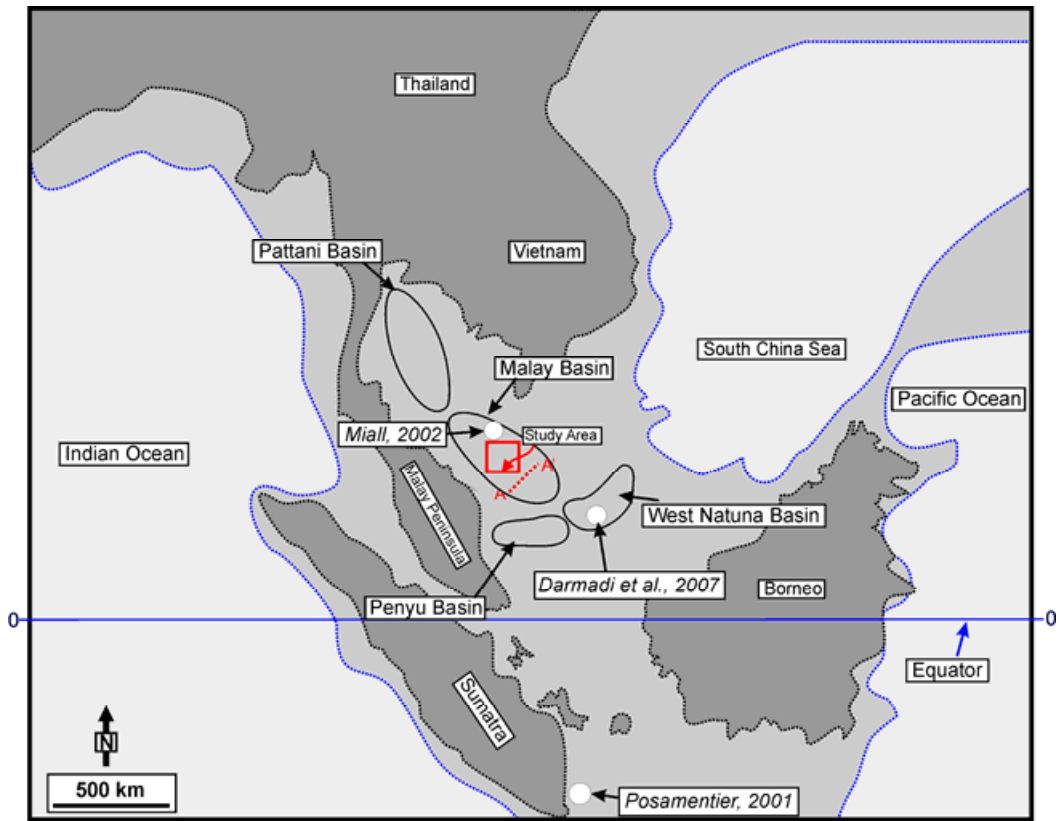
**Table 6**

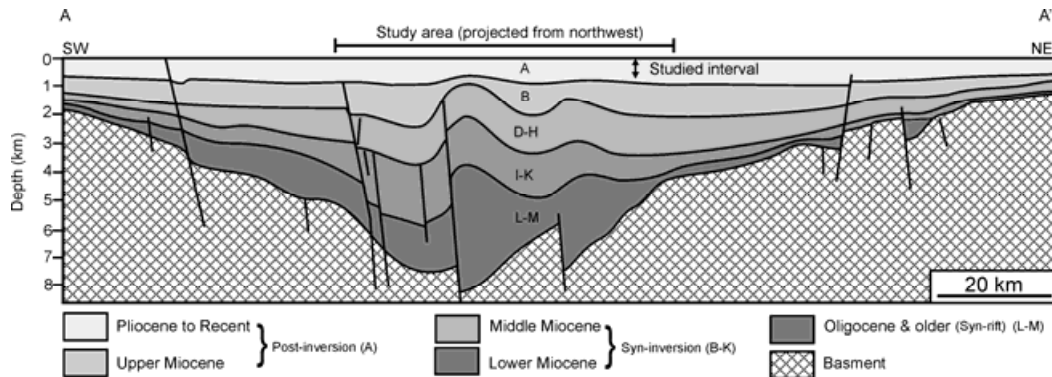
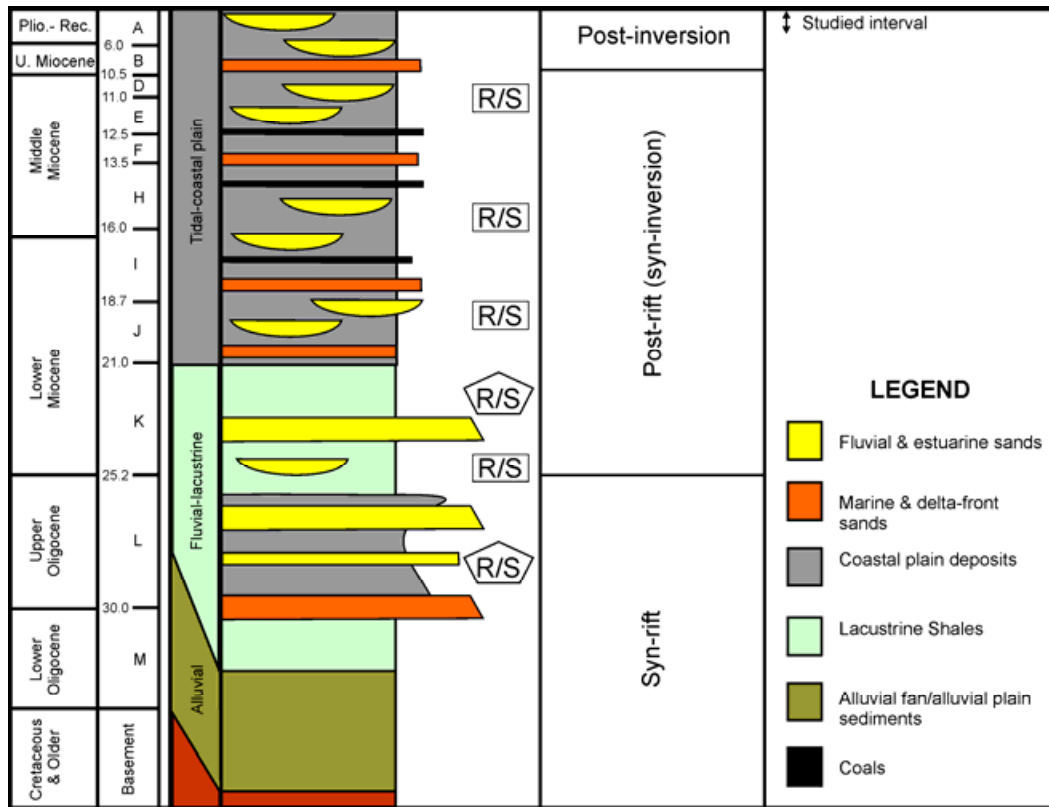
<b>No</b>	<b>System</b>	<b>Drainage basin (km<sup>2</sup>)</b>	<b>Vw (m)</b>	<b>Vd (m)</b>	<b>A (m<sup>2</sup>)</b>	<b>Shelf gradient (m/km)</b>	<b>Reference</b>
<b>1</b>	<b>La Batre</b>	75	1065	11	6000	0.63	Mattues & Rodriguez (2007)
<b>2</b>	<b>Magnolia</b>	111	522	7	2200	0.63	Mattues & Rodriguez (2007)
<b>3</b>	<b>Fish</b>	427	862	12	5750	0.63	Mattues & Rodriguez (2007)
<b>4</b>	<b>Lavaca</b>	6778	5523	18	37800	0.76	Mattues & Rodriguez (2007)
<b>5</b>	<b>Calcasieu</b>	10339	2781	24	32000	0.40	Mattues & Rodriguez (2007)
<b>6</b>	<b>Sabine</b>	29616	4235	13	44400	0.39	Mattues & Rodriguez (2007)
<b>7</b>	<b>Nuecces</b>	49002	3710	22	44000	1.20	Mattues & Rodriguez (2007)
<b>8</b>	<b>Trinity</b>	53573	16594	22	97500	0.44	Mattues & Rodriguez

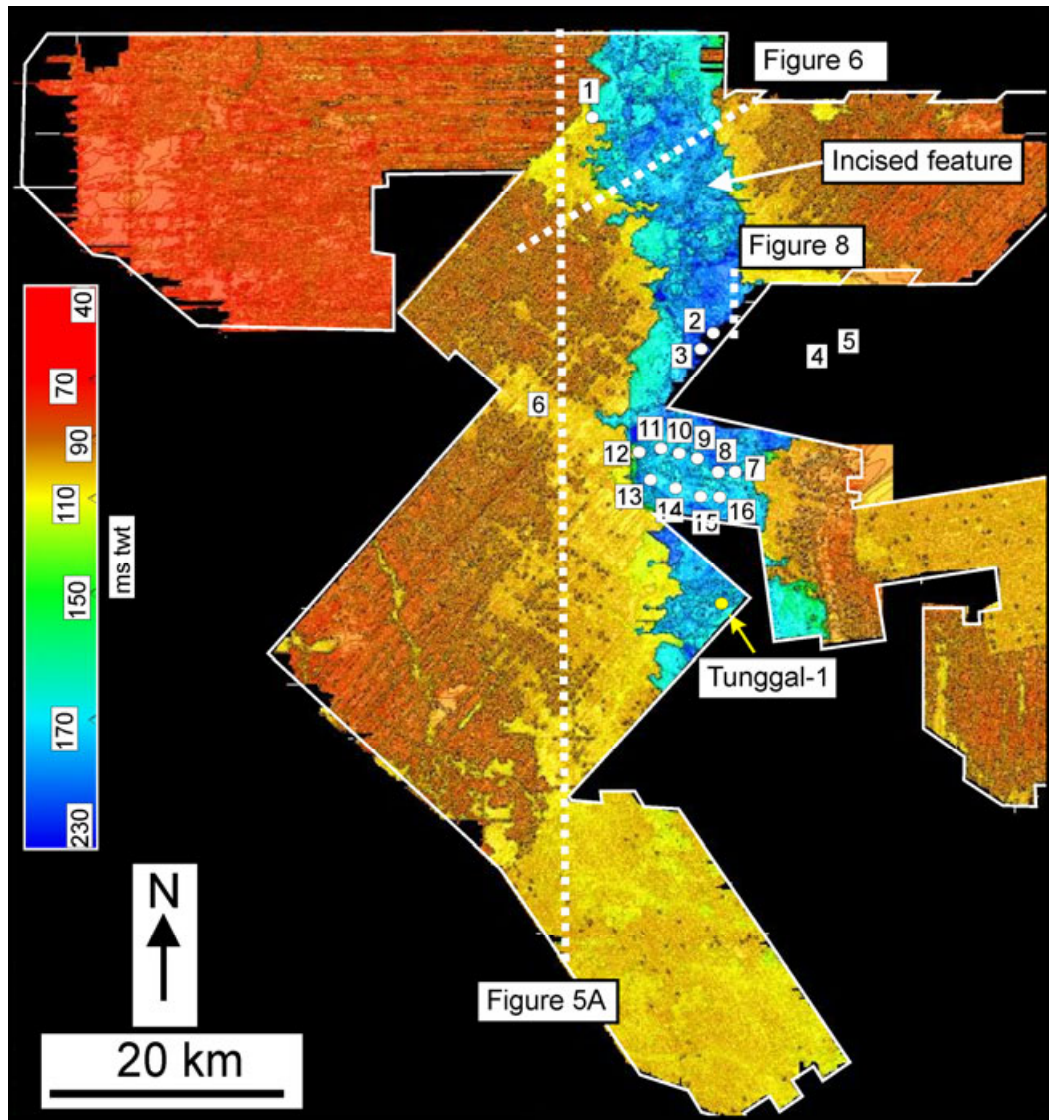
---

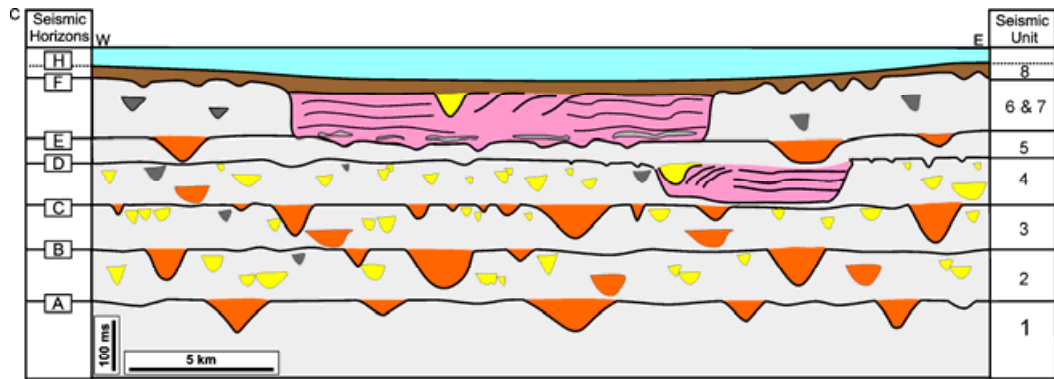
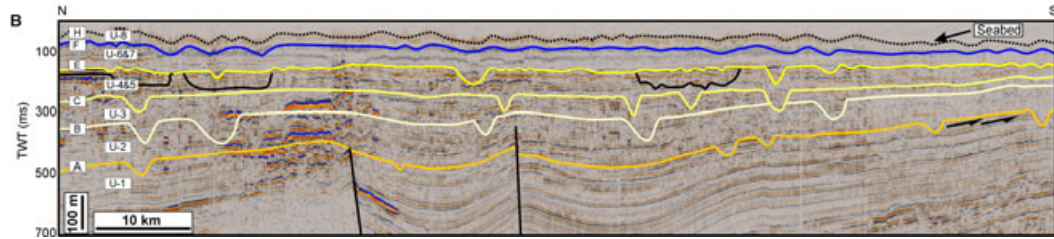
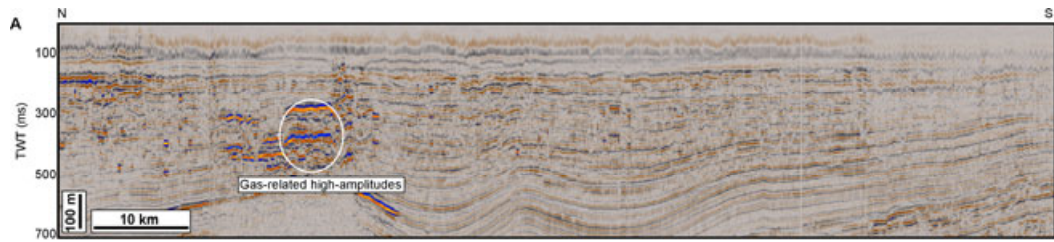
							(2007)
<b>9</b>	<b>Mobile-Tensaw</b>	133552	14304	19	201000	0.63	Mattues & Rodriguez (2007)
<b>10</b>	<b>Palaeo-Chao Pahraya</b>	<b>1350000</b>	<b>135000</b>	<b>71</b>	<b>958500</b>	<b>0.01</b>	<b>Present study</b>
<b>11</b>	<b>New Jersey (smallest)</b>	---	100	1	100	0.0001	Nordfjord et al. (2005)
<b>12</b>	<b>New Jersey (largest)</b>	---	1800	25	4000	0.01	Nordfjord et al. (2005)

---









- Straight to low-sinuosity channels
- Sea water
- Coastal plain deposits
- Moderate-sinuosity channels
- Major incised valleys
- Holocene marine mud
- High-sinuosity channels



